Available online at www.sciencedirect.com

ScienceDirect

Journal of Magnesium and Alloys 12 (2024) 443–464

www.elsevier.com/locate/jma

Review

Microstructure design of advanced magnesium-air battery anodes

Xu Huang[a], Qingwei Dai[a,*], Qing Xiang[b], Na Yang[a], Gaopeng Zhang[a], Ao Shen[a], Wanming Li[c]

[a] School of Metallurgy and Materials Engineering, Chongqing University of Science and Technology, Chongqing 401331, China
[b] School of Materials and Architectural Engineering, Guizhou Normal University, Guiyang 550025, China
[c] School of Material and Metallurgy, University of Science and Technology Liaoning, Anshan 114051, China

Received 6 September 2023; received in revised form 6 November 2023; accepted 24 January 2024
Available online 22 February 2024

Abstract

Metal-air battery is an environmental friendly energy storage system with unique open structure. Magnesium (Mg) and its alloys have been extensively attempted as anodes for air batteries due to high theoretical energy density, low cost, and recyclability. However, the study on Mg-air battery (MAB) is still at the laboratory level currently, mainly owing to the low anodic efficiency caused by the poor corrosion resistance. In order to reduce corrosion losses and achieve optimal utilization efficiency of Mg anode, the design strategies are reviewed from microstructure perspectives. Firstly, the corrosion behaviors have been discussed, especially the negative difference effect derived by hydrogen evolution. Special attention is given to the effect of anode micro-structures on the MAB, which includes grain size, grain orientation, second phases, crystal structure, twins, and dislocations. For further improvement, the discharge performance, long period stacking ordered phase and its enhancing effect are considered. Meanwhile, given the current debates over Mg dendrites, the potential risk, the impact on discharge, and the elimination strategies are discussed. Microstructure control and single crystal would be promising ways for MAB anode.

Keywords: Magnesium; Air battery; Anode; Microstructure; Anodic efficiency.

1. Introduction

With the intensification of the climate warming, increasing consumption and demand for energy, the shift from fossil fuels to clean energy is of great importance to alleviate resource scarcity and carbon emissions [1,2]. Given the intermittent nature of wind and solar energy, reliable electrochemical energy storage systems have always been significant and desirable [3,4]. Admittedly, lithium-ion (Li-ion) battery played a key role over the past several decades. However, with the expectation of high energy density performance, Li-ion battery has been somewhat sluggish in further performance improvement. Another point is that the short life Li-ion battery inevitably leads to serious environmental problems such as water and soil pollution. And high-cost Li as a strategic metal, may face the risk of shortage in the coming decades as a strategic metal [5–7]. Therefore, it is necessary to establish new storage systems, and find the replacement of Li anode.

Recently, the metal-air battery has considered to be the ideal energy storage system. Due to its excellent theoretical discharge performance and clean production characteristics, it has attracted many researchers (Fig. 1(a)). The metal-air battery is composed of the metal anode, the catalyst-loaded air cathode, and the electrolyte, as shown in Fig. 1(b). As the metal-air battery running, the metal ion M^+ generated by the oxidation of the metal anode, then moves in the electrolyte and reacts with the O_2 of the cathode to generate current with metal oxide products formed [8].

The intuitive advantage of the metal-air battery is that the oxygen in the atmosphere is directly utilized as an oxidant, reducing system weight, and avoiding CO_2 emissions. The strong discharge activity of the metal anodes is necessary to ensure the high energy storage potential of the air battery. The light metal magnesium (Mg), with high theoretical specific capacity (2205 mAh g^{-1}) and low reduction potential (−2.37 V

* Corresponding author.
E-mail address: daiqingwei@cqust.edu.cn (Q. Dai).

https://doi.org/10.1016/j.jma.2024.01.025

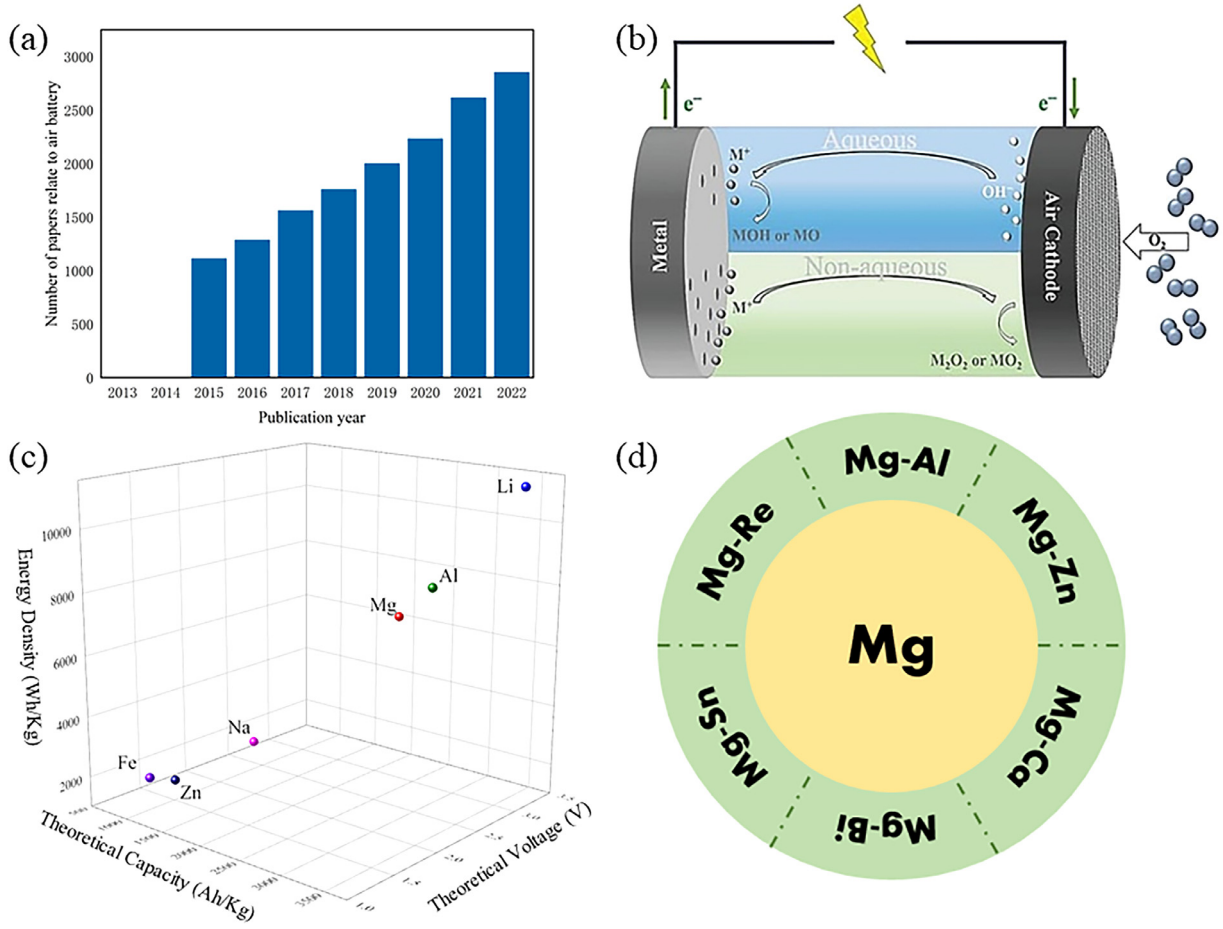

Fig. 1. Schematic diagram of: (a) the numbers of papers related to air battery, based on web of science. (b) The metal-air battery. Reproduced with permission [9]. (c) the performance of various anodes of metal-air battery. (d)the Mg alloys for air battery anode.

vs. SHE), is an ideal anode candidate. Unfortunately, the Mg-air battery (MAB) is still in the laboratory stage due to the high polarization and corrosion susceptibility of the Mg anode. Most of the Mg matrix are consumed by the corrosion without generating any current, the actual discharge capacity and specific energy density are far below expectations, resulting mainly in low anodic efficiency [10,11]. Therefore, researchers have done a lot of work to criticize MAB technology and provide strategies for further improvement. Li et al. [12] reviewed the historical progress of MAB and analyzed the reaction mechanisms. Zhang et al. [13] and Zhang et al. [14] summarized the progress of typical cathode catalysts and non-noble metal electrocatalysts of MAB.

Previous work has mostly focused on improving kinetics of oxygen reduction reaction of MAB. At present, there is little critical discussions on the anode of MAB, especially the effect of microstructure on anodic efficiency is ignored. This review focuses on the design strategies of MAB anode as microstructure perspectives.

1.1. Ideal candidate

Among various metals, Mg and its alloys are favored in the research of air battery anodes due to their excellent electrochemical performance (Fig. 1(c,d)). The standard negative electrode potential of Mg is lower than that of aluminium (Al) [15]. As the candidate to replace Li anode, the abundant and low-cost Mg anode is less prone to dendrite formation during the discharge process, reducing the risk of fire and explosion [16,17]. Dendrite is also the difficulty in zinc-air battery research [18,19]. Compared with sodium-air battery and iron-air battery, MAB can avoid the formation of complex discharge products and the deformation of electrode in alkaline environment [20–23].

Poor corrosion resistance is always the main factor limiting the application of Mg anodes. Although high-purity Mg may have a low corrosion rate compared to Mg alloys with impurities and noble second phases, it is not an appropriate choice for MAB anode. It tends to exhibit high discharge voltage and low anodic efficiency at low current density, while low discharge voltage and high anodic efficiency at high current density. And the strong anodic hydrogen reaction of high purity Mg anode leads to the low anodic efficiency directly [24,25]. Apart from designing pure Mg anode with specific micro/nano-structure used for air battery, the evolution of microstructure caused by forming process and alloying strategies has been noted by researchers.

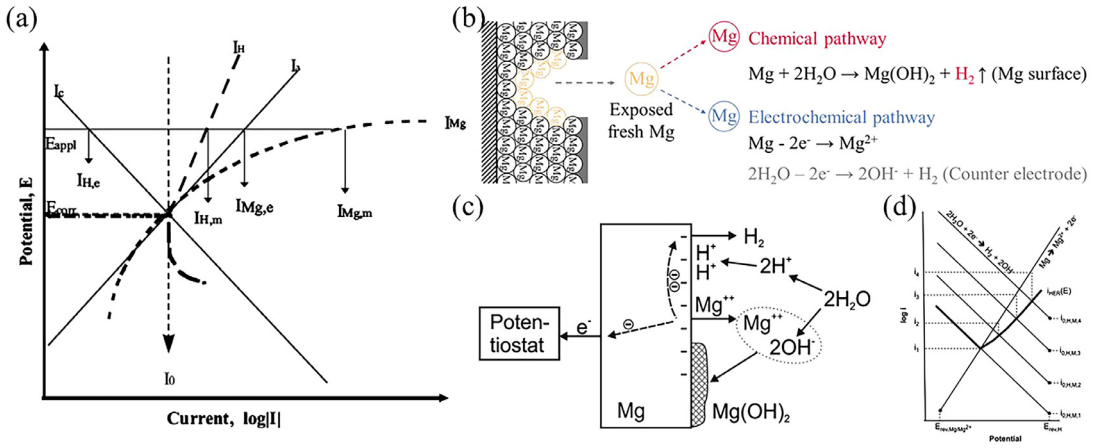

Fig. 2. Schematic diagram of: (a) the NDE. Reproduced with permission [26]. (b) The anodic polarization. Reproduced with permission [30]. (c) The model to explanate the NDE by Bender et al. Reproduced with permission [28]. (d) The HER changes with potential, and the exchange current density of HER changes with dissolution rate. Reproduced with permission [31].

1.2. Negative difference effect

The poor corrosion resistance of Mg is mainly due to the weak protection provided by the passive layer. While acting as the MAB anode, the self-peeling of the passive layer ensures the contact between the Mg matrix and the electrolyte, thus maintaining the discharge activity. However, the hydrogen evolution reaction, the parasitism of corrosion progress, is not honorable. As the degree of polarization caused by the oxygen concentration is low, and hydrogen evolution occurs before oxygen absorption, the negative difference effect (NDE) occurs. That is, the hydrogen evolution intensifies with the increase of the MAB anode potential, as shown in Fig. 2(a), which further causes additional mass loss and reduces the anodic efficiency [26,27]. It is currently believed that there are two hydrogen evolution pathways, local dissolution within the corrosion pit and reduction of H_2O on the passivated surface outside the pit. And there are two cathode processes that dominate the NDE, external polarization and H^+ enrichment, respectively [28,29].

This process involves the transition from cathodic hydrogen evolution to anodic hydrogen evolution [32]. Currently, the discussion of cathodic hydrogen evolution dominated by monovalent Mg^+ is extensive, and Chen et al. [25] proposed that discharge behavior of Mg anode is also based on the Mg^+ mechanism. It is assumed that Mg is oxidized to Mg^+ by anodic reaction and then reacts with H_2O to generate hydrogen. However, as an unstable intermediate, Mg^+ cannot be detected, and its existence is still controversial. Zhang et al. [30] reported that the chemical reaction between the Mg anode interface and the electrolyte drives the hydrogen evolution, as shown in Fig. 2(b). Mg is more likely to transfer one electron to form Mg^+ during the anodic oxidation process, than to simultaneously transfer two electrons to form Mg^{2+}. However, it has not been confirmed that Mg^+ can attract the second electron to instantly form equilibrium stable Mg^{2+}, or undergo further chemical reactions with other substances in the system. Atrens et al. [33] considered that if the NDE is dominated by Mg^+, the lifespan of Mg^+ must be long enough and able to react with other chemicals. Meanwhile, Frankel et al. [31] observed that the total amount of hydrogen evolution decreases with increasing current density, which is different from the theoretical value generated by the same amount of Mg^+. It shows the direct oxidation of Mg to Mg^{2+} caused by the anode current, as shown in Fig. 2(c). And the amount of Mg^{2+} generated by the applied anode current is greater than the value predicted by Faraday's law, and significantly increases the hydrogen evolution volume [34]. Based on the model of H^+ discharge established by Bender et al. [28], as shown in Fig. 2(d). The strong hydrogen evolution behavior by anodic polarization is the main reason for the intensification of the H^+ discharge.

The Mg^+ dominant mechanism is also based on the porous composite surface layer, which ensures the transfer of the polarization current. Due to the local anodic dissolution of Mg, uneven passive layers are formed. The hydrogen evolution at the Mg anode is generated by chemical reactions between the Mg surface and the electrolyte, depending on the exposed Mg matrix. Anodic polarization promotes the formation and inward-growth of internal MgO at the film/Mg interface, as in Eq. (1), which can be highly fractured due to its small volume compared to Mg. Thus, with the increasing anodic potential, the porosity of the film increases, further hydrogen evolution and NDE intensifies [30,35].

$$MgO + H_2O \rightarrow Mg(OH)_2 \quad (1)$$

Compared to the corrosion current density, the negative effect of the hydrogen evolution reaction on the anodic efficiency of MAB is more significant. It is attributed to the anodic efficiency, which is directly determined by the hydrogen evolution reaction during anode polarization instead of the corrosion current density [36]. The actual weight loss caused by NDE is much higher than the theoretical value corresponding to the current applied during the discharge process. The main strategies to weaken NDE are the addition of corrosion inhibitors or the development of dual liquid electrolytes,

while ignoring the influences of the microstructure of the Mg-air battery anode.

1.3. Design considerations

Discharge capacity and anodic efficiency have always been the primary considerations for MAB. While the side corrosion process during Mg discharge is the inevitable nightmare for researchers [24]. The commonality between the corrosion process and the discharge process is that Mg loses two electrons and oxidizes to Mg^{2+}. However, there are fundamental differences in the mechanism of the two processes. The total corrosion process of Mg is shown in Eq. (2), the anode and cathode reactions are shown in Eqs. (3) and (4), respectively.

$$\text{Total}: Mg + 2H_2O \rightarrow Mg(OH)_2 + H_2 \quad (2)$$

$$\text{Anode}: Mg - 2e^- \rightarrow Mg^{2+} \quad (3)$$

$$\text{Cathode}: 2H_2O + 2e^- \rightarrow 2OH^- + H_2 \quad (4)$$

The corrosion process involves hydrogen evolution reaction and oxygen reduction reaction, which may dissolve at the self-corrosion potential. As the electrons transferred to the cathode and formed a current path, the discharge reaction occurs. The total, anode, and cathode processes are shown in Eq. (5) ~ (7), respectively.

$$\text{Total}: Mg + 1/2O_2 + H_2O \rightarrow Mg(OH)_2 \quad (5)$$

$$\text{Anode}: Mg - 2e^- + 2OH^- \rightarrow Mg(OH)_2 \quad (6)$$

$$\text{Cathode}: 1/2O_2 + H_2O + 2e^- \rightarrow 2OH^- \quad (7)$$

From Eq. (2), (5) and Fig. 3(a), the electrons released by the corrosion process are mainly reduced by H_2O to produce hydrogen on the anode surface, rather than being transferred to the cathode to form a current path [37,38]. This explains why no current is generated. The corrosion loss of the Mg matrix leads directly to a significant reduction in anodic efficiency. And the corrosion/discharge products adhere on the anode interface, preventing the transfer of Mg^{2+} and leading to anode polarization. In particular, as the potential is mainly determined by the sequential electrochemical adsorption of hydroxide to the Mg anode surface, the deposition of discharge products may lead to potential disturbances during discharge [39,40]. Furthermore, the hydrogen evolution reaction tends to accompany the corrosion process and induce NDE [11,24], as shown in Fig. 3(b). Therefore, more attention should be paid to the microstructure on the corrosion resistance and anodic efficiency of MAB anodes.

Combined with the forming experience of Mg anode [41–43], the grain size and orientation of Mg anode can provide optimized choices for air battery. The corrosion anisotropy related to grain orientation has been confirmed, while the discussion on the electrochemistry is rare, especially the comprehensive consideration of corrosion resistance and anodic efficiency as an air battery. The form and detachment trends of corrosion/discharge products are also related to the structural defects like twins and dislocations [44]. In addition to the refinement and modification of the microstructure, the targeted introduction of the long period stacked ordered (LPSO) phase can significantly improve the discharge activity. Based on recent discussion, unexpected microstructures such as dendrites may occur during the discharge, which cannot be ignored. In conclusion, the microstructure evolution of Mg anode should be emphasized in the design of advanced air batteries with high corrosion resistance and anodic efficiency.

2. Poor corrosion resistance, low anodic efficiency?

Since the most of Mg matrix is converted to undischarged corrosion products during the discharge process, the main method used to calculate anodic efficiency is based on the theoretical and actual weight loss ratio of the discharged MAB anode [11,45–47], as Eq. (8).

$$\text{Anodic Efficiency}(\%) = W_{theo}/\Delta W \times 100\% \quad (8)$$

Where ΔW is the weight loss of the MAB anode during discharge, and W_{theo} is the theoretical weight loss. Thus, it is assumed that the MAB anode with poor corrosion resistance may have low anodic efficiency, generally. However, in the study of two crystal characteristics, the relationship between two performances is delicate. One is the grain boundary effect caused by grain size, and the other is the chunk effect anisotropy contributed to the grain orientation dependent behavior.

2.1. Grain boundary effect

In general, refining the grain size of Mg anodes can improve ion transport performance and achieve high electrochemical activity of the air battery [4]. It is a favored strategy to introduce alloying elements as nucleation sites to limit grain growth. However, the relationship between the grain size and corrosion resistance of Mg and its alloys has always been controversial, with the main contradiction being whether highly active grain boundaries can suppress corrosion propagation. As grain refinement increased, the density of grain boundaries increases, and the intergranular corrosion may occur along the grain boundaries. Impurities tend to accumulate at the grain boundaries, inhibiting the formation of passive layers. Thus, the corrosion products layer on the Mg alloy with ultra-fine grains may be loose, and has the poor corrosion resistance compared to the Mg alloy with coarse grains. When the intergranular corrosion spreads to certain oriented grains, it further tends to transform into intragranular corrosion [48–55].

However, the products layer, which tends to detach, is necessary to maintain the discharge activity of MAB. And the grain boundary free energy also determines the electronic properties of the agglomerated particles of the polycrystalline compounds. The high energy grain boundary decomposes preferentially to the grain interior. As the grain refinement increases, the proportion of total atoms near or at the surface

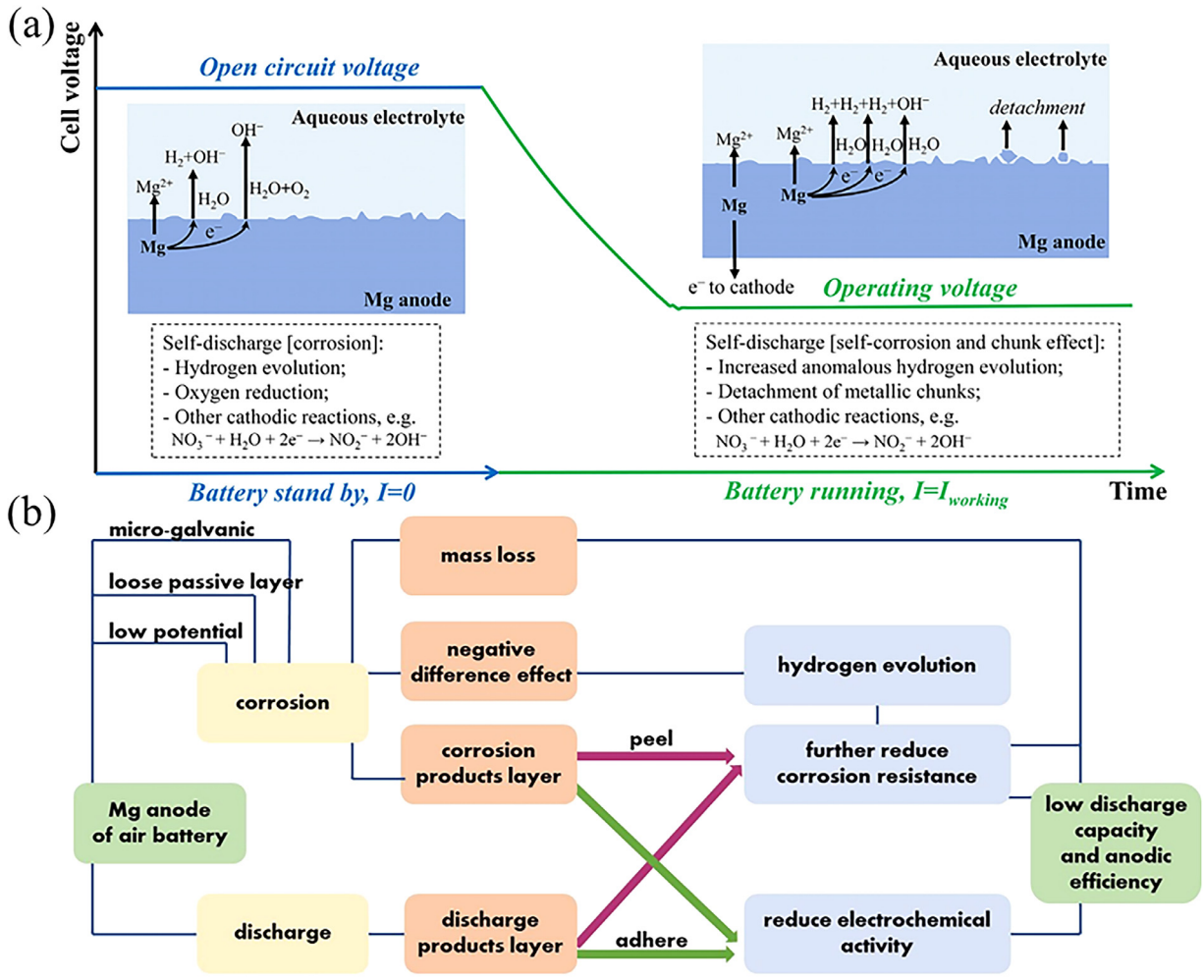

Fig. 3. Illustration of: (a) the corrosion and discharge processes of Mg battery anodes. Reproduced with permission [38]. (b) The considerations for designing anodes for MAB.

increases, resulting in high electrochemical reaction activity, which significantly improves the anodic efficiency of the Mg-air battery [56–59]. Yang et al. [60] suggested that the influence of grain boundaries on corrosion and discharge processes is similar in degree. In addition, some studies have shown that increased grain boundary can suppress hydrogen evolution during discharge by reducing the cathode/anode ratio. Strongly active grain boundary can be considered as anode and form micro-galvanic with low energy grain area, which may preferentially dissolve [61–63]. Acceleration of anodic kinetics improves the anodic efficiency and discharge activity, as shown in Fig. 4(a,b).

The fine-grained structure of Mg anodes ensures that uniform dissolution during discharge [64], and many researchers aim to obtain fine-grained MAB anodes by plastic deformation. Forming processes such as equal channel angular extrusion [65], friction stir processing [66], and homogenization treatment before extrusion [67], are used to refine metal anodes of air battery. Some external field treatments are also aimed at refining the anode grain size of Mg-air battery. Chen et al. [68] refined the anode grain size to one-tenth by ultrasonic field vibration, and the optimum discharge capacity and anodic efficiency of Mg-air battery were increased to 1417 mAh g^{-1} and 63.3%, respectively.

In addition, introducing alloying elements can limit grain growth, and improve the cell voltage of Mg-air battery. Taking samarium (Sm) element as an example, the relationship between grain size and cell voltage is shown in Fig. 5(a). However, few elements introduced only refine the grain size without forming a new phase in the alloying. When calcium (Ca) is introduced, the grain size of Mg-Ca anodes is refined by increasing the Ca content. However, it also causes the aggravation of the micro-galvanic effect with the increase of the Mg_2Ca phase, resulting in the corrosion acceleration and voltage disturb [40], as shown in Fig. 5(b). Similarly, although the grain size of Mg-Bi anode gradually decreases with the increase of Bi content, the increase of Mg_3Bi_2 phase and (0001) texture content further deteriorates the discharge performance of MAB [69]. However, when Ca and Bi are added to Mg anode, the grain effect is stronger than the phase effect. Although the unfavorable Mg_2Bi_2Ca phase existed, the discharge performance of Mg-Ca-Bi anode can be improved by

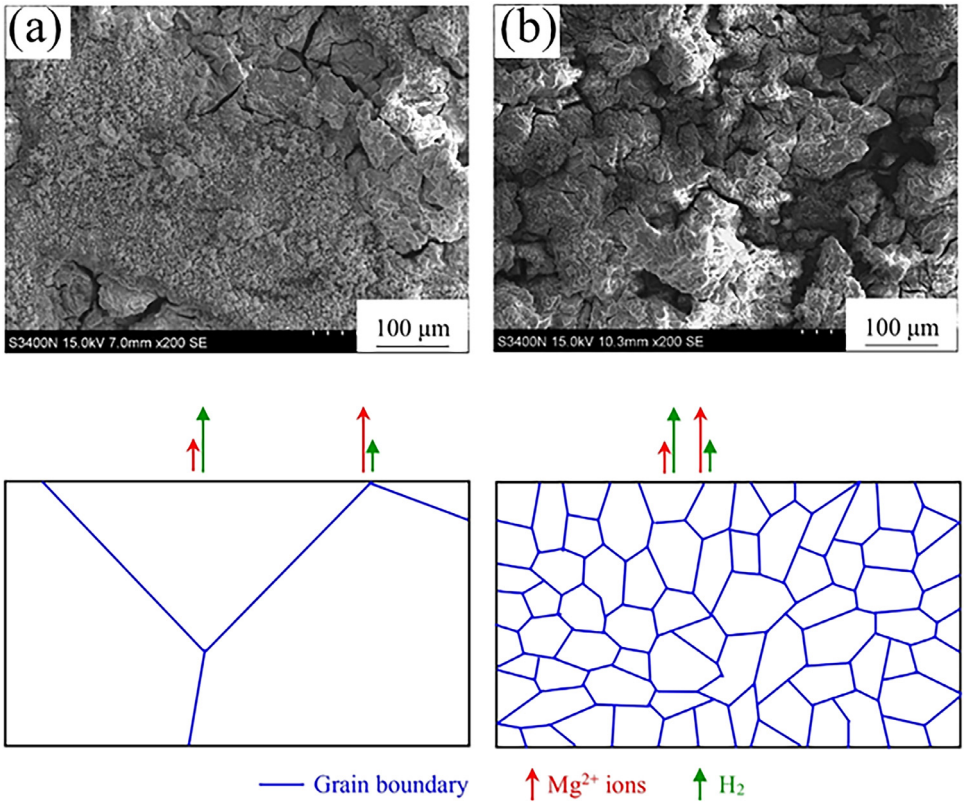

Fig. 4. Corresponding schematic of anodic dissolution and hydrogen evolution of Mg-air battery with different grain size anodes: (a) grain sizes of 472.89 ± 154.31 μm, and (b) grain size of 667.28 ± 291.35 nm. Reproduced with permission [62].

the refined grains and non-basal texture [70]. In conclusion, grain size is a critical factor to be considered and grain refinement can be an effective way to improve the discharge performance of MAB. On the other hand, the anode performance of MAB is influenced by several microstructural factors, which need to be discussed comprehensively. In particular, the effects of grain orientation and second phase on MAB cannot be ignored, and will be discussed in the next sections.

2.2. Chunk effect anisotropy

The discharge performance of the Mg-air battery depends on the local surface reactions. Since each grain is embedded in the matrix in a random orientation and exhibits corrosion and electrochemical anisotropy, the grain orientation of the Mg anode has been considered as one of the determining factors for the air battery [72]. The (0001) basal texture has the high positive potential and low anodic polarization compared to the prismatic texture. And the structure of the passive layer on the basal texture is dense [73,74], it is considered to have better corrosion resistance. The grain orientation-dependent corrosion behavior is influenced by the effect of the solute and dislocation density, the area fraction of each orientation, and the orientation related corrosion rate jointly [75].

Atomic density should be considered first. The grain orientation determines the atomic arrangement on the metal surface, and the density of the atomic arrangement further determines the surface energy. The anodic dissolution rate of Mg is related to the surface energy, i.e., the energy of Mg^{2+} escaping from the metal lattice and dissolving into the electrolyte [76,77]. It exhibits an incomplete inverse proportional function to atomic density, and the matrix is difficult to dissolve at low surface energy [39,78]. Liu et al. [79] calculated the surface energy of different grain orientations based on atomic density, and as speculated, the (0001) textured surface has the lowest surface energy. The anodic dissolution of Mg is also related to the dissolution of the $Mg(OH)_2$ product layer and the adsorption kinetics of OH^-. The densely packed surface with coordination saturation is weaker in binding to OH^- compared to the loose surface and tends to suppress anodic dissolution during discharge. Meanwhile, the high energy surfaces tend to adsorb H_2O or H^+, exacerbating hydrogen evolution and NDE. This may also explain why the (0001) basal texture surface has high conductivity compared to the prismatic texture [39,78,80].

However, the corrosion resistance and anodic efficiency do not exhibit complete positive correlation in this situation. The basal texture's inherent electrochemical activity is weak, and the stable passive layer hinders electrons transfer between the matrix and electrolyte, leading to the inferior discharge performance compared to the prismatic texture. Yang et al. [81] studied Mg-Al-Zn Mg alloy anodes with four angled surfaces. As the (11–20) and (10–10) prismatic oriented grains increased, and the (0002) oriented grain decreased, the cor-

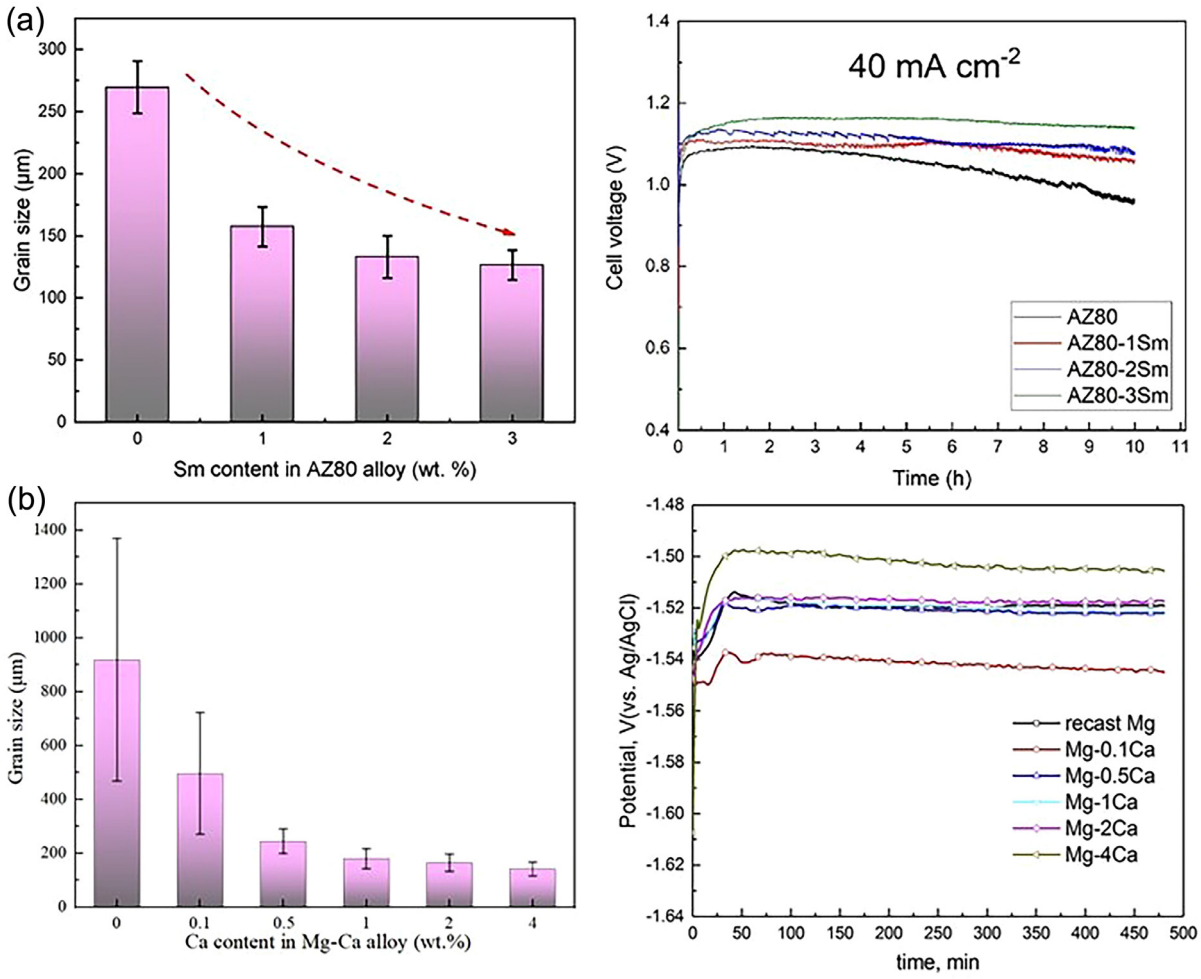

Fig. 5. Schematic of grain size, and discharge performance of: (a) AZ80 with different content Sm. Reproduced with permission [71]. (b) Pure Mg with different content Ca. Reproduced with permission [40].

rosion current density and corrosion rate increased from 8.6 μA cm^{-2} and 0.2 mm y^{-1}, to 93.2 μA cm^{-2} and 2.13 mm y^{-1}, respectively. It is noteworthy that the anodic efficiency of the prismatic texture is 67.6%, which is higher than that of the basal texture, standing at 60.7%. This strange phenomenon is also observed in an air battery that employs an extruded diluted Mg-Sn-Zn-Ca anode. The transversal surface (TS) with prismatic texture exhibits inferior corrosion resistance and higher anodic efficiency during discharge, as compared to the longitude surface (LS) with basal texture [82], as shown in Fig. 6. No controversy is that the dissolution kinetics of prismatic texture are strong, thus increased content can boost discharge activity [60]. However, the discrepancy in corrosion resistance and anodic efficiency across various textures requires further discussion.

Wang et al. [83] suggested that the prismatic texture can promote uniform dissolution of the Mg-air battery anode, as shown in Fig. 7. This theory was confirmed by the work of Yang et al. [84], which showed that Mg-Sn-Y anode of air battery with basal texture tends to dissolve unevenly during discharge. And the uniformly dissolved prismatic texture tends to inhibit the detachment of undischarged large particles or matrix, known as the "chunk effect". This may explain why the high corrosion resistance of the basal texture leads to low anodic efficiency. However, it should be noted that this phenomenon usually occurs at low current densities. By increasing the current density, the anodic efficiency difference between the basal texture and the prismatic texture can be reduced and even reversed [83]. It can be attributed to the hydrotalcite ($Mg_6Al_2(OH)_{16}CO_3{\cdot}4H_2O$,) preferentially formed and then transformed to the $Mg(OH)_2$ and Al_2O_3 products at high current density, and the uniformity of Mg anode consumption increases with increasing current density [85,86], thus the "chunk effect" usually occurs at low current density.

The corrosion resistance and anodic efficiency of various textures of the Mg-air battery are included in Table 1. This study examines the influence of texture on the anodic efficiency of the Mg air battery as well as its comprehensive consideration with corrosion resistance (J_{corr} represents corrosion current density, E_{corr} represents corrosion potential). The focus is not solely on corrosion resistance in different cor-

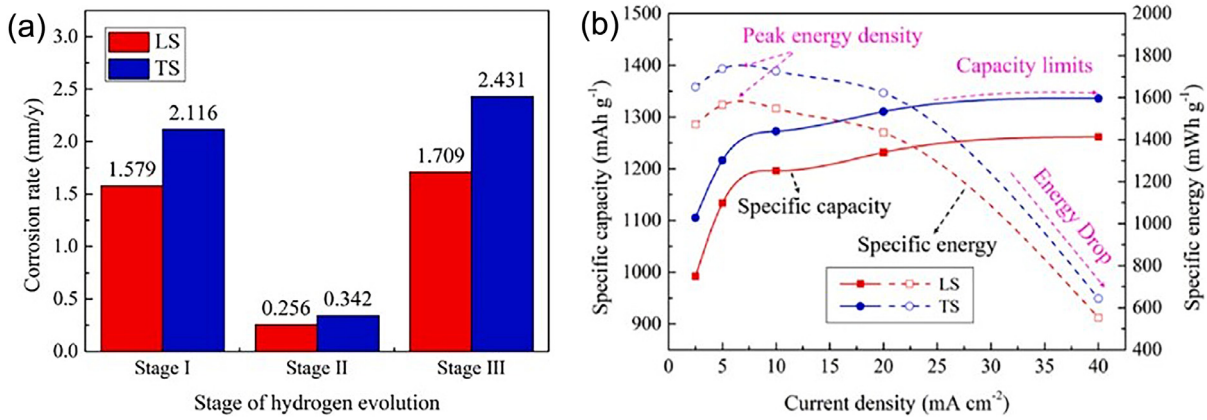

Fig. 6. (a) Hydrogen evolution, (b) specific capacity and specific energy of the Mg-Sn-Zn-Ca anode with different surfaces. Reproduced with permission [82].

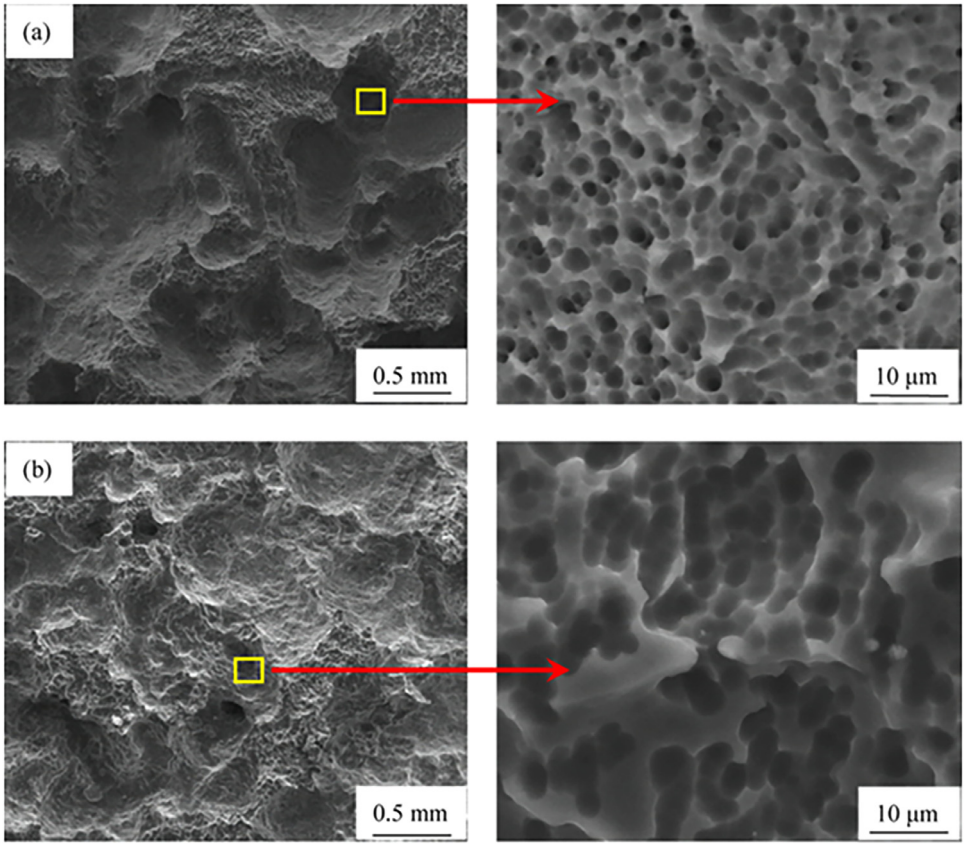

Fig. 7. Discharged morphologies of AP65I without products: (a) rolling surface, (b) cross-section surface. Reproduced with permission [83].

rosion environments. The experimental conditions for each group are consistent, and representative applied current density is selected.

Previous findings have shown the collaborative influence of grain size and orientation. Specifically, when the extruded Mg-air battery anode is further rolled, the basal texture strengthening can decrease the corrosion rate. However, the improvement in anodic efficiency may be attributed to the more significant grain refinement effect [74].

3. Discussion on the microstructure characteristics

3.1. Phase features

The type and content of alloying elements are critical to the corrosion and discharge performance of MAB anodes. The formation of new phases is always the key factor in alloy design. It is well known that the noble phases can form micro-galvanic with the α-Mg matrix, and this accelerates

Table 1
Corrosion and anodic efficiency of MAB anodes with different texture.

Mg electrode	Work surface	E_{corr} (vs. SCE)/V	J_{corr}/(μA cm^{-2})	Current density/ (μA cm^{-2})	Anodic efficiency/%	Ref
Rolled Mg-Al-Pb	rolling surface	−1.571	24.3 ± 4.2	10	37.1 ± 0.6	[83]
					41.5 ± 0.7	
	cross-section surface	−1.537	90.7 ± 19.2	180	84.3 ± 1.3	
					80.6 ± 1.6	
Extruded Mg-Al-Zn	ED-TD 0°	−1.428	8.6	40	60.7	[81]
	ED-TD 30°	−1.454	15.3		62.3	
	ED-TD 60°	−1.484	39.1		65.3	
	ED-TD 90°	−1.553	93.2		67.6	
Rolled Mg-Al-Zn	rolling surface	/	/	10	65.7	[87]
	cross-section surface				71.3	
Extruded Mg-Sn-Zn-Ca	longitude surface	−1.563	43.8	40	57.7	[82]
	transversal surface	−0.1.593	73.3		59.6	
Extruded Mg-Bi	Basal texture 14.2%	/	/	20	57.3 ± 1.5	[69]
	Basal texture 22.5%				56.0 ± 3.0	
	Basal texture 27.8%				55.5 ± 2.2	

the corrosion of the low potential Mg matrix as a sacrificial anode. However, the potential difference is not the only factor determining the corrosion process. Although the low potential phases are preferentially subject to suffer corrosion, they cannot protect the Mg matrix, but instead deteriorate the corrosion resistance. And the high potential phases as specific morphologies, can inhibit corrosion diffusion. For example, the Mg_2Ca phase is preferentially corroded as an anode in Mg-Ca alloys, while the corrosion channels left at grain boundaries can promote the penetration of corrosive ions into the Mg matrix and reduce the corrosion resistance. On the other hand, the $Ca_2Mg_6Zn_3$ phase, which has the highest potential compared to the α-Mg matrix and the Mg_2Ca phase in the Mg-Zn-Ca alloy, can hinder the continuous distribution and corrosion of the Mg_2Ca phase by reducing the proportion, which improves the corrosion resistance, as shown in Fig. 8(a). The anodic efficiency of Mg-2Zn-1Ca anode of air battery can reach 60% at high current density [88,89]. And although some phases deteriorate the corrosion resistance of the Mg anode, they can improve other electrochemical properties. For example, Mg_3Hg particles in Mg-Hg anode can worsen the micro-galvanic effect, while improving the peak voltage and effective discharge time [90]. Thus, the role of second phases in the corrosion and discharge process needs to be fully considered.

Recently, several studies have investigated new types of Mg anodes incorporating various components for MAB, and have reported promising results. Notably, Xiao et al. [91] developed a novel $Mg_{64}Zn_{36}$ (at.%) anode using a single-phase design for air batteries, as shown in Fig. 8(b). This anode exhibited a high anodic efficiency of 94.8 ± 4.9%, surpassing any previously reported MAB anodes. In this section, the discussion progresses to the effects of different phases on MAB anodes, rather than introducing Mg alloys as MAB anodes.

3.1.1. Mg-X alloy

The addition of tin (Sn) promotes the conversion of columnar grains to dendrites, while also reducing the secondary dendrite arm spacing as the content increased. In the electrolyte, Sn has a tendency to form SnO_2 on the anode surface, whereby segregated Sn along the dendrite region transforms into (α-Mg+Mg_2Sn) eutectic phase. Whenever the discharge process take place, microcracks generally appear on the SnO_2 surface layer and near the grain boundaries, which enhances the detachment of discharge products. However, excessively Sn content leads to the high potential Mg_2Sn phase intensifying the micro-galvanic effect as cathode. This, in turn, increases the resistance of SnO/SnO_2 composite layer, which weakens electrochemical activity [46,92–94]. Additionally, the Mg anode's discharge pore is small because of high Sn content [95]. Furthermore, the increased Sn content leads to a decrease in the basal texture and an increase in prismatic texture. The (0002) oriented grains in the Mg-0.7Sn-1.4Y MAB anode had almost disappeared [84]. According to Bao et al. [96], the addition of Ca to Mg-Sn anode resulted in the formation of an (α-Mg + CaMgSn) eutectic structure, which caused cracks on the product layer through phase modulation, thereby contributing to stable voltages. Le et al. [97] observed that Mg-Sn-Ca anode with a low Sn/Ca mass ratio may exhibit the best discharge performance as air battery.

While adding rare-earth (RE) elements to Mg anode is anticipated to enhance the discharge capabilities of MAB, the surface enrichment of RE (such as zirconium) element and the presence of Mg_xRE_y phases may enhance the NDE effect [98,99]. Ma et al. [100] discovered that alloying 5 wt.% lanthanum (La) into Mg can form the $LaMg_{12}$ phase, which features a reticular microstructure that hinders the laterally extended corrosion and promotes uniform dissolution. As the content of La increases, a large-area noble $LaMg_{12}$ phase

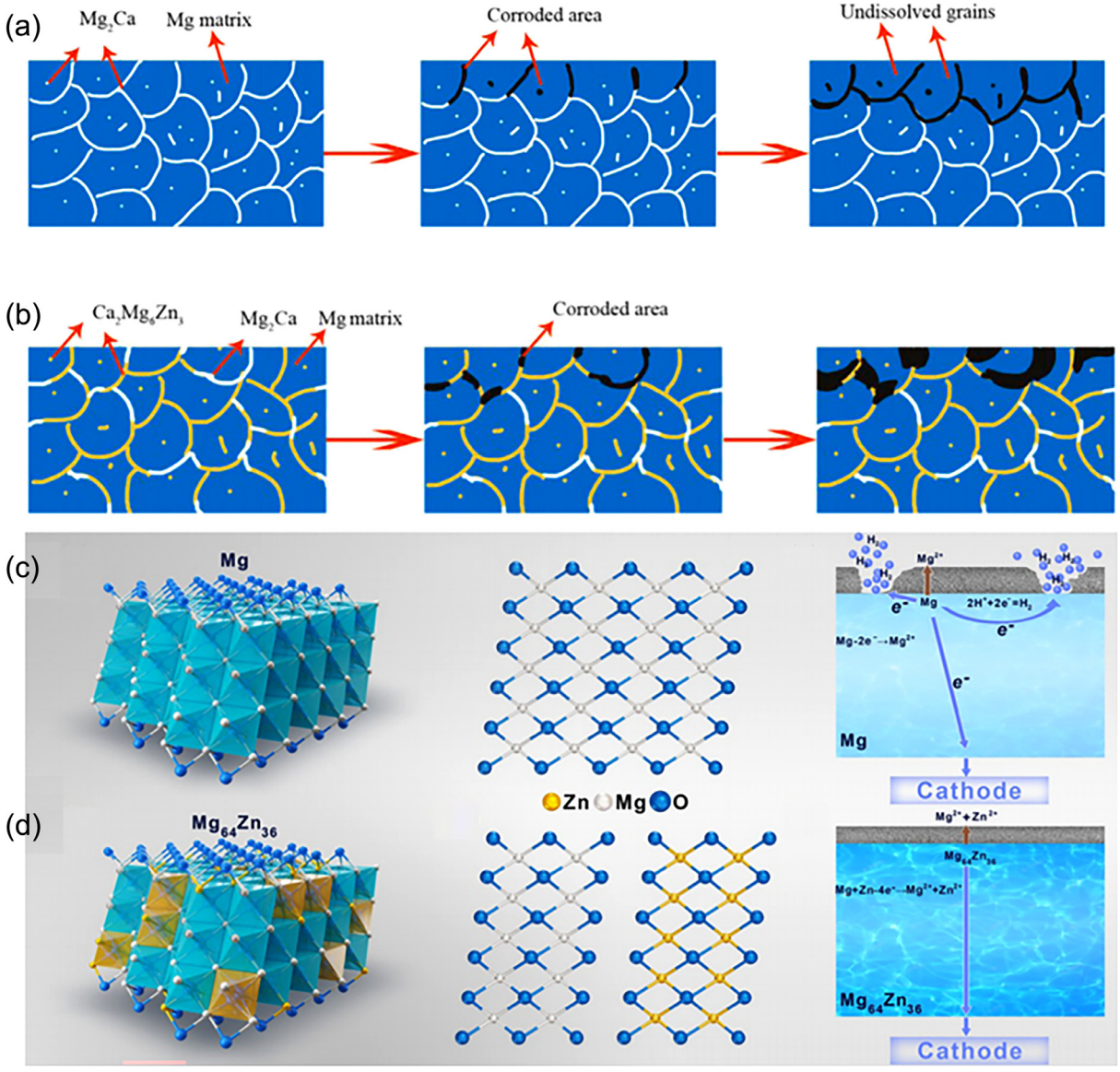

Fig. 8. Schematic illustrations of the microstructure and discharge process: (a) Mg-1Ca, (b) Mg-2Zn-1Ca. Reproduced with permission [88], (c) pure Mg, and (d) $Mg_{64}Zn_{36}$. Reproduced with permission [91].

forms, which accelerates the corrosion process of the Mg matrix through micro-galvanic effect. As previously discussed, the Mg_2Ca phase in Mg-Ca anodes, and the Mg_3Bi_2 phase in Mg-Bi anodes also accelerate the corrosion of Mg. The micro-galvanic corrosion between the matrix and new phases are key factors that must not be ignored in the alloying design of MAB anodes. Recently, Chen et al. [101] states that the energy density of the Mg-Ge anode in air batteries is 37% higher than that of ultra-high-purity Mg. This is because Germanium (Ge) tends to form the Mg_2Ge eutectic phase at grain boundaries. The dissolution of Mg_2Ge can create cavities with a Ge-relevant film covering.

The introduction of Al element with three valence electrons into the Mg anode is conducive to refine the grain and improve discharge voltage. Additionally, due to its high hydrogen overvoltage, it suppresses the passivation of the Mg anode by peeling away the $Mg(OH)_2$ product layer, and hence, improves the discharge activity of MAB [102]. Considering both cost and the favorable properties of corrosion resistance and mechanical properties, Mg-Al alloy anodes are the preferred choice for air battery technology. However, it is essential to the acknowledge the effect of β-$Mg_{17}Al_{12}$ phase. On the one hand, larger volume fractions of the β-$Mg_{17}Al_{12}$ phase, with a continuous distribution, can act as a barrier to inhibit corrosion diffusion. Conversely, when the β-$Mg_{17}Al_{12}$ phase is scattered under a small volume fraction, it can act as a high potential cathode, which accelerates galvanic corrosion [103,104]. Fig. 9 shows that, when compared to the granular and cluster second phases of hot-rolled (HR) AZ91(Mg-9Al-1Zn, wt.%), those of die-cast (DC) AZ91 exhibit a network structure which possess better corrosion resistance and discharge performance [105]. As a result, the addition of ele-

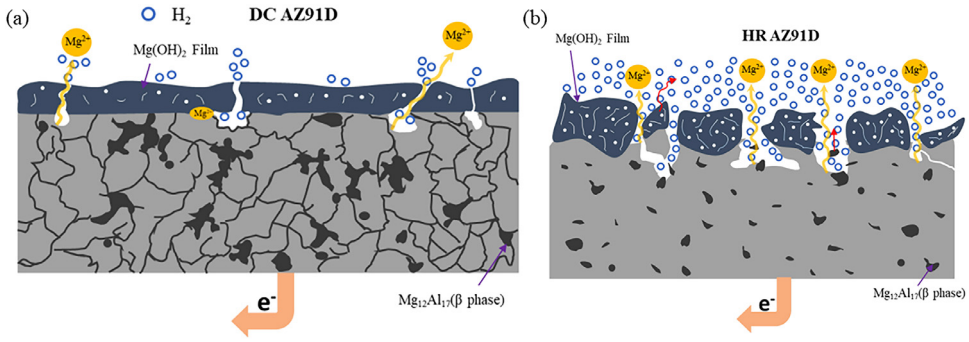

Fig. 9. Schematic model of the AZ91D air battery anodes discharged: (a) die-cast, (b) hot-rolled. Reproduced with permission [105].

ments introduced to modify the second phase can be a critical strategy for enhancing air battery performance, and this is a common objective achieved by most alloying techniques, with the exception of grain refinement.

3.1.2. Mg-Al-X alloy

Introducing Zn into Mg-Al alloys promotes uniform anode consumption, and improves tolerance for heavy metal impurities [85]. As Al content increases, the dispersion of the β-$Mg_{17}Al_{12}$ phase at grain boundaries tends to interfere with the stability of the passive. Consequently, AZ91 anodes demonstrate more pronounced discharge activity than AZ61 (Mg-6Al-1Zn) and AZ31 (Mg-3Al-1Zn) [92,106]. Modification of the β-$Mg_{17}Al_{12}$ phase can enhance the activation of the matrix surface, improve corrosion resistance, optimize anodic efficiency, and enhance discharge activity [107]. For example, Wang et al. [108] demonstrated that introduced Cd in AZ61 can modify the β-$Mg_{17}Al_{12}$ phase from punctate to chain. This modification increased discharge capacity from nearly 675 to 1004 mAh g^{-1}, anodic efficiency from nearly 24.5% to 41.8%, and corrosion current decreased from 15.2 $\mu m\ cm^{-2}$ to 1.3 $\mu m\ cm^{-2}$.

The addition of an appropriate amount of manganese (Mn) element can enhance the corrosion resistance of the Mg-Al anode. Furthermore, Al tends to combine with Mn to form spherical $Al_{11}Mn_4$ and polygonal Al_8Mn_5 particles. Zheng et al. [109] obtained a Mg-6Al-1Sn-0.4Mn (wt.%) anode using orthogonal design for air battery, with discharge potential averaging reaching at −1.602 V (vs. SCE). In Mg-Al-Ca alloys, the fine Al_2Ca particles act as cathode in micro-galvanic reactions, leading to worsened corrosion resistance and reduced discharge capacity despite grain size refinement [40,110]. Zou et al. [111] investigated the effect of adding barium (Ba) in to Mg-Al anode. At 0.4 wt.%, grain refinement and inhibition of cathodic hydrogen evolution occurred, whereas at 0.7 wt.%, $Al_{13}Ba_7$ phase formed and corrosion process accelerated. Thus, it is important to avoid the formation of binary intermetallic particles with noble potential acting as the cathode of micro-galvanic corrosion, with particular consideration given to the Al-X compound [45].

The introduction of lead (Pb) into Mg-Al anodes does not result in the formation of new phases containing Pb, which tends to dissolve in the matrix. However, Pb has a synergistic effect with Al in accelerating the decomposition and precipitation of products. That is, the PbO on the surface promotes the precipitation of $Al(OH)_3$, and then $Al(OH)_3$ promotes the detachment of the $Mg(OH)_2$ product layer by forming $2Mg(OH)_2$-Al(OH) under the activation interface mechanism. Representatively, the AP65 (Mg-6Al-5Pb, wt.%) alloy has become the iconic MAB anode, which is usually used as a benchmark for evaluating high-performance MAB anodes [36,64,112]. Unfortunately, its fouling characteristics and high cost potentially limit its application [41]. The further introduced In in the Mg-Al-Pb alloy also tends to dissolve without forming new phase. While it promotes the small area precipitation of β-$Mg_{17}Al_{12}$ phase by mutual repulsion with Al atoms, dispersed β-$Mg_{17}Al_{12}$ and grain refined are conducive to the uniform dissolution of the Mg matrix, which can weaken the “chunk effect”. Meanwhile, In^{3+} can deteriorate the formed of the passive layer, so that deposited In on the matrix can inhibit the adhesion of discharge products. Thus, it accelerates the activation process during the initial discharge stage and enhances the electrochemical activity under high current density conditions. However, the continuous increase of In content can lead to the re-deposition of In, and the lattice distortion promotes the growth of β-$Mg_{17}Al_{12}$ phase. Meanwhile, the adsorption of Cl^- by In favors to the formation of corrosion pits, which may be preferential sites for hydrogen evolution and result in the reduction of electrochemical activity [63,107,113,114]. Feng et al. [115] replaced In with La in the Mg-Al-Pb-In anode, and improved the cycle life at 10 mA cm^{-2}. Alternatively, the addition of Ce in the AP65 MAB anode can purify the Mg anode by reducing impurities with grain size refinement. Al and Ce can form to Al_4Ce phase, Al_2Ce phase, and even $Al_{11}Ce_3$ phase with slight β-$Mg_{17}Al_{12}$ precipitation. Large volume Al_4Ce can act as a barrier to inhibit corrosion diffusion. And it also promotes the products layer to peel off from the surface with loose and porous structure, thus improving the anodic efficiency and discharge activity [104,116–118]. The effect of Y is similar to that of Ce. Except for grain refinement, Y preferentially forms negative potential Al_2Y specie with Al, and aggregates into small sizes γ phase distributed uniformly in the matrix. As a result, the Al content of β-$Mg_{17}Al_{12}$ decreases, and the morphology becomes spherical, which can achieve long service life under stable anodic efficiency [64,119].

When the RE elements are added individually into Mg-Al alloys, Al is preferentially combined with RE elements. This inhibits the formation and expansion of the β-$Mg_{17}Al_{12}$ phase. La preferentially combines with Al to form a network of Al_2La phase, which can weaken the chunk effect and NDE by promoting uniform dissolution [120,121]. As for samarium (Sm), the Al_2Sm phase is formed and exists three crystal matching relationships with the α-Mg matrix. It can refine the β-$Mg_{17}Al_{12}$ phase and matrix grain size as a nucleation site during solidification. However, the granular Al_2Sm phase tends to agglomerate at high Sm content. And $Al_{11}Sm_3$ particles can be formed at high Al content, which can increase the parasitic anodic hydrogen reaction rate [71,122]. It is worth noting that the single addition of Sm or La to the AZ31 alloy can actually reduce the voltage of battery, while the addition of a small amount of Sm and La to the AZ31-Ca alloy can increase the discharge voltage. This can be attributed to the formation of Al_2Ca particles, which can hinder grain boundary migration and act as potential nucleation sites for recrystallized grains. The lattice mismatch between Ca and Mg also leads to significant lattice strain near grain boundaries, resulting in the weak oxygen intensity and thin discharge product layer at the sites of Al_2Ca particles. As Sm and La are present at appropriate contents, Al_2Ca and polygonal Al_2RE particles inhibit the generation of potential Al-Mn phases. These particles collectively stimulate anode kinetics by micro-galvanic as weak cathodes, and promote the rupture of discharge products to ensure contact between the electrolyte and the matrix. However, excessive Al_2RE particles may exacerbate local dissolution of the Mg matrix by consuming Ca solute [45,80,123,124]. Incidentally, anode kinetics can be improved by controlling the Ca content and distribution of the Mg_2Ca phase [125]. At low Ca content, a small number of Mg_2Ca particles are distributed within the grains. At high Ca content, the eutectic structure is composed of α-Mg and multiple Mg_2Ca present at grain boundaries and inter-dendritic regions. The highly active Mg_2Ca phase promotes the formation of micro-anode sites, which can accelerate the intergranular electrochemical process. As the Mg_2Ca phase is refined to nanoscale and continuously distributed, it is conducive to the deposition of surface passive layer, which may reduce the electrochemical activity [40,45,126]. Further, as for the introduction of rare-earth Gd, there is a competition of priority formation between Al_2Gd and β-$Mg_{17}Al_{12}$ phase. Cubic Al_2Gd particles can weaken hydrogen evolution and local corrosion at low current densities by forming the protective layer. With increasing Gd content, it changes from coexisting to a single needle-like structure Gd_2Mg phase associated with the α-matrix. It refines the β-$Mg_{17}Al_{12}$ phase to promote uniform dissolution of Al elements in the matrix. It is effective to reduce internal resistance of the air battery, and further reducing the voltage loss due to the increased current density at the load, resulting in optimal anodic efficiency and electrochemical activity [42,120,127,128]. In addition, RE alloying can also modify the discharge morphology. Compared to AZ80, AZ80-La-Gd has a smooth surface and fine pits, which promotes the contact between matrix and electrolyteand thus maintains discharge activity [120].

Gadolinium (Ga) and Gd can provide high specific capacitance for Mg storage with high hydrogen overpotential. The low lattice expansion rate and diffusion barrier can more easily promote the diffusion of Mg^{2+}. Meanwhile, the noble valence cations can deteriorate the stability of the passive layer by combining with discharge products. Ga is enriched at the front of the liquid phase, leading to undercooling of the components to provide nucleation sites and inhibit the growth of the separated eutectic. When the Ga content reaches 4wt.%, the Ga_2Mg phase is formed [129–132]. Zou et al. [132] reported that the surface of AZ80–2.5Ga anode exhibits regular and uniform, and the optimum discharge capacity is 25% higher than that of AZ80 anode. Ga is also attempted to be added to Mg-Hg anode, the $Mg_{21}Ga_5Hg_3$ phase may generate less charge transfer resistance in the faradaic reaction, and adjust the electro-negativity discrepancy between the α-Mg matrix and the Mg_3Hg [133].

3.1.3. Mg-Li-X alloy

With the exception of Mg-Al based alloys, Mg-Li-Al alloys usually have uniform distribution of AlLi particles. This can weaken the negative influence by the high electrochemical activity β-Li phase, and leading to an improvement in the discharge voltage and capacity. As an active site, AlLi tends to peel off in clusters during the discharge process. Additionally, the discharge products layer, which is dominated by soluble LiOH tends to form microcracks in order to maintain the discharge activity. Fine particles of AlLi and $MgLiAl_2$ with negative potential dominate the dissolution process, weakening the micro-galvanic effect and protecting the α-matrix as a sacrificial anode [36,134,135]. Ma et al. [136] suggested that the Mg-Li-Al-Ce alloy, primarily composed of Li_3Mg_7 and Al_2Ce phases, shows promise as a MAB anode due to its low self-corrosion rate and hydrogen evolution. Owing to discharge products layer's loose structure and crack defects, the discharge activity surpasses that of Mg-Li-Al and Mg-Li anodes in succession, resulting in anodic efficiency of 85.2%.

The addition of Zn element with high solid solubility is beneficial for the uniform dissolution of Mg-Li-Al air battery anodes [137]. However, there is a content peak, excessive Zn may form large volume fractions of high potential Mg_7Zn_3 and Mg_4Zn_7 phases, which improve micro-galvanic as the cathodes [103,138]. Lin et al. [139] studied the air battery anodes of Mg-Li-Al-Zn alloy with different Al contents. As the Al content increases, the number of AlLi particles also increases significantly. These fine active particles tend to transform into Al particles densely embedded in the $Mg(OH)_2$ passive layer with a high volume fraction during corrosion, which may reduce the electrochemical activity of MAB. Further, the RE elements Ce and Y can also improve the electrooxidation activity of Mg-Li based MAB anodes [102]. Wang et al. [137] combined the properties of the above elements and constructed the Mg-Li-Al-Ce-Y-Zn anode composed of advantageous AlLi, Al_2Ce, Al_2Y, $Mg_{24}Y_5$, and MgCe phases. While Zn is dissolved in β-Li, which can inhibit local anodic disso-

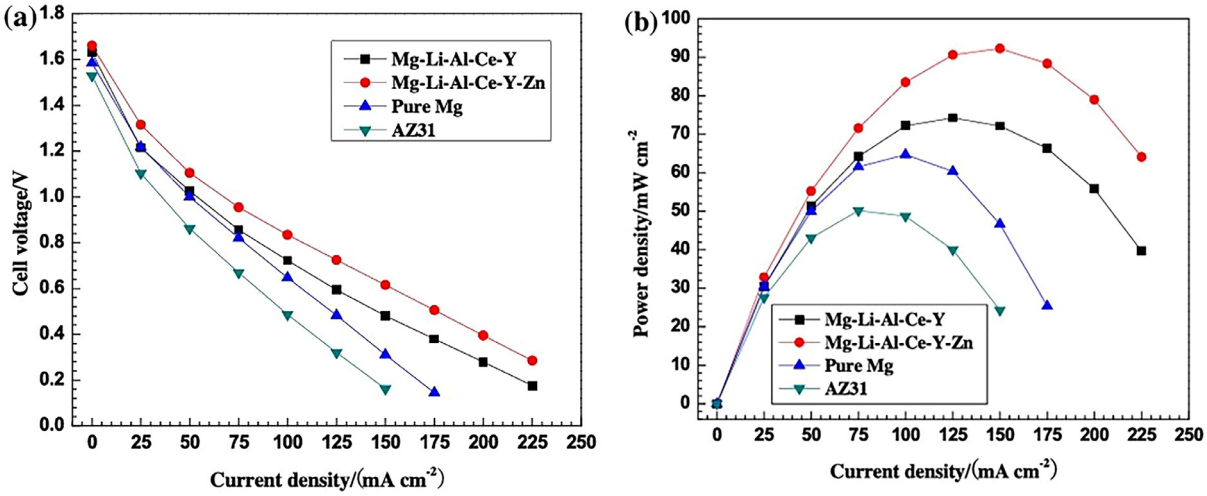

Fig. 10. Performance of Mg-air batteries with pure Mg, AZ31, Mg-Li-Al-Ce, and Mg-Li-Al-Ce-Y anode: (a) cell voltage, (b) power density. Reproduced with permission [137].

lution by reducing the potential difference, and the hydration of Zn^{2+} accelerates the destruction of the product layer by reducing the environmental pH near the surface [103]. Whether at the low current density, which is prone to the "chunk effect", or at the high current density up to 180 mA cm^{-2}, the Mg-Li-Al-Ce-Y-Zn anode all have the excellent anodic efficiency and peak power density, comparable to Mg-H_2O_2 semi-fuel cells [137], as shown in Fig. 10.

3.2. Crystal structures

Mg-Li alloy is considered revolutionary and environmentally friendly anode for MAB, boasting excellent discharge capacity [138]. The crystal structure of Mg-Li anodes is dependent on the content of Li, and subsequently impacts the anode performance of MAB. When the Li content exceeds 5.7 wt%, the hexagonal stacked Mg-Li anode will gradually form into a dual phase alloy by precipitating α-Mg phase, like the Mg-8Li based anode contains α-Mg and β-Li fibers. When the Li content is increased to 10.3 wt.%, the α-Mg phase disappears completely, and the crystal transforms into the body centered cubic structure with only the β-Li phase remaining, like Mg-11Li based anode, which has attempted in MAB [137,140,141].

Due to the formation of soluble discharge products (LiOH) by Li, loose composite product layer on the Mg anode tends to peel off, improving the electrochemical activity. The theory of the large current density promotes the uniform dissolution of Mg anodes, which is also applicable to MAB with containing only β-Li. When exposed to a large current density, the previous dissolute β-Li phase of the Mg anode transforms into particle-like clusters, resulting in a finely discharged surface that weakens the NDE effect and possesses a depolarization effect [134,139,141], as shown in Fig. 11(a-e). According to Liu et al.'s [134,141] researches, Mg-11Li anode exhibits optimum discharge capacity of 1478 mAh g^{-1} and anodic efficiency of 62.1% at 40 mA cm^{-2}. Furthermore, the anode exhibits a power density of up to 58.9 mW cm^{-2} at 80 mA cm^{-2}, as shown in Fig. 11(f).

In addition, the grain size and orientation are affected by the Li content, and the extruded Mg-1Li alloy prefers to form the basal texture. As the Li content increases, the grain size decreases, and the ratio of recrystallization decreases. Eventually, it transforms into the prismatic texture (Li $\geq$ 3) [142].

3.3. Crystal defects

High twins and dislocation densities tend to accelerate the anodic dissolution of MAB. As topical crystallographic defect sites, twisted lattice at these locations makes atoms susceptible to corrosion. And high activation energy drives hydrogen evolution, and increases the self-corrosion rate [143]. Therefore, twins and dislocations of Mg anode may affect MAB performance negatively, which need to evaluate the processing methods and propose improvement measures.

The effect of twins on the MAB anode is controversial and depends on the type, energy, and volume fraction [144]. Huang et al. [145] reported that AZ31 anode of air battery with twins has higher discharge voltage and a shorter retardation time. Gerashi et al. [146] considered that the high energy twin region provides the preferred corrosion site with more protective products layer. At present, most of the works aim to eliminate the negative effect of twins on Mg corrosion resistance [49,69,147]. Yan et al. [49] stimulated twinning nucleation and refined low-energy twins by multi-directional compression treatment, which avoids the adverse effect of non-equilibrium grain boundaries, and suppresses the micro-galvanic by modifying the distribution of the second phase. Twins-mediated dislocation mediated by twins dominates the deformation process, with grain orientation being the crucial determinant of the ductility and the plastic deformation mechanism of twins. Each formed dislocation formed is influenced by grain orientation [148,149]. During dissociation or phase transformation, dislocations significantly affect corrosion dif-

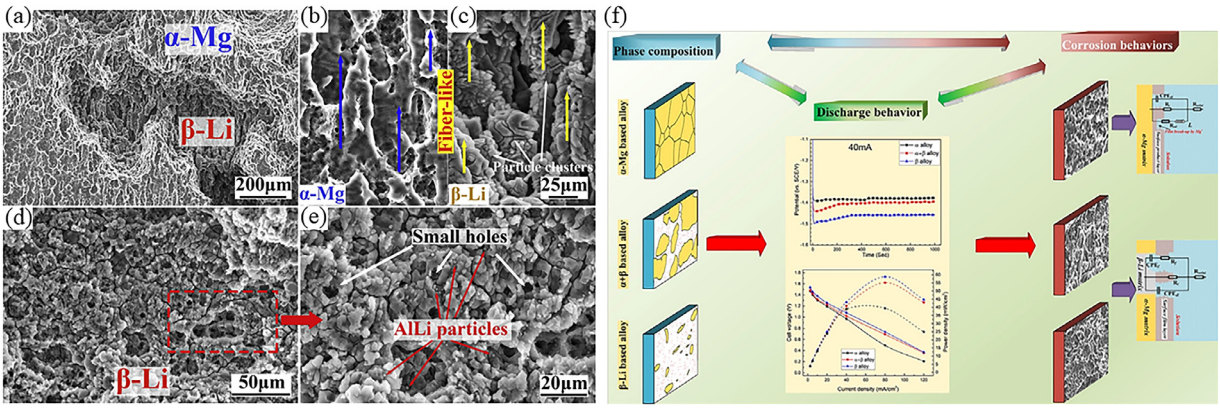

Fig. 11. Discharged surface morphologies of Mg anodes with discharge products removed: (a-c) $\alpha+\beta$ based Mg anode, (d-e) β based Mg anode [134]. And (f) Phase composition, discharge behavior, and corrosion behaviors of Mg anodes with different constitutions [141].

fusion as reaction sites for matrix dissolution [150]. This effect is similar to dislocation disorder introduced by grain refinement, which improves the corrosion resistance of Mg alloys. The distorted lattice makes atoms more active, resulting in the matrix always preferentially dissolving at dislocation sites [151,152]. The deformation energy of dislocations may decrease the potential of the α-Mg matrix, and weaken the potential difference between the anode and cathode. Consequent to this effect, it weakens the driving force for electron transport. In addition, corroded dislocation sites with priority are more susceptible to the growth of the $Mg(OH)_2$ layer, which ultimately leads to the reduction of the active electrode area [36,150,153]. The process of dynamic recrystallization involving grains with extension twins has been found to increase, leading to the formation of an ordered region between the twins and grain boundaries. As a result, grain boundary energy is weakened and corrosion resistance is improved [154]. This may be conducive to improve the anodic efficiency of MAB. Some works reduced the twins and dislocation density by hot rolling or heat treatment, which improved the discharge performance of MAB anode [57]. Wang et al. [62] obtained the anode of MAB with small grain size, weak basal texture, low dislocation density, and dispersed nanoscale second phase by spark plasma sintering. Moreover, the homogenization treatment before extrusion is beneficial to weaken the dislocations, promote the growth of dynamic recrystallized grains, and uniform distribution of nanoscale precipitates [67]. The dissolution process of α-Mg matrix during discharge is shown in Fig. 12. These processes lay the foundation for the high discharge capacity and anodic efficiency of MAB.

4. Specific designs

4.1. LPSO phase for enhancement

Long period stacked ordered (LPSO) intermetallic compounds are present in Mg alloys that containing Zn and RE such as Y, Gd, etc. The LPSO phase can enhance not only strength and ductility, but also dynamic recrystallization through particle stimulated nucleation mechanisms. This strengthening phase enable grain refinement of the MAB anodes [155]. The typical LPSO phases in Mg-Zn-Y alloy include 18R (rhombohedral) and 14H (hexagonal) configurations [156]. The "R" type represents an even number of α-Mg layers separating the building blocks, while the "H" type represents an odd number. Both configurations can be transformed through heat treatment [157].

Zhang et al. [158] precipitate LPSO phase and $Mg_3Y_2Zn_3$ phase in the Mg-2Zn-Mn anode by adding Y. As Y content increases, the micro-galvanic between these phases and the α-Mg matrix weakened due to phase distribution characteristics. Chen et al. [159] conducted a T6 heat treatment to transform the α-Mg matrix of the Mg-Gd-Zn air battery anode into the 14H LPSO phase, as shown in Fig. 13(a,b). The results indicate that it displays a remarkable discharge capacity and anodic efficiency while maintaining stable discharge voltage at low and high current densities, as shown in the Fig. 13(c,d). The corrosion resistance of a suitable volume fraction LPSO phase with high potential is primarily attributed to its barrier effect, which overrides the cathodic galvanic effect. In contrast, the weak potential difference exerts a positive influence by exciting the discharge process and enhancing the anodic kinetics. To put it simply, the distribution and volume of LPSO phase dictate its impact on corrosion behavior [160]. Due to the low potential of the α-Mg matrix, it's inevitably dissolved before the LPSO phase as contacting with electrolyte. However, the initial corrosion film formed on the LPSO phase and the α-Mg matrix differs in properties. The corrosion resistance of the LPSO phase is inferior to that of the α-Mg matrix. Through heat treatment, the transformation of the α-Mg matrix into the LPSO phase weakens the inherent galvanic effect and the negative impact of the second phase [161]. As a result, the initial corrosion can be divided into two stages: the preferential dissolution of the α-Mg matrix upon initial contact with the electrolyte, and the preferential dissolution of the LPSO phase after the formation of the passive layer on the α-Mg matrix in an extremely short period of time. During discharge, the layered LPSO phase is prone to be peeled away with the discharge products. This

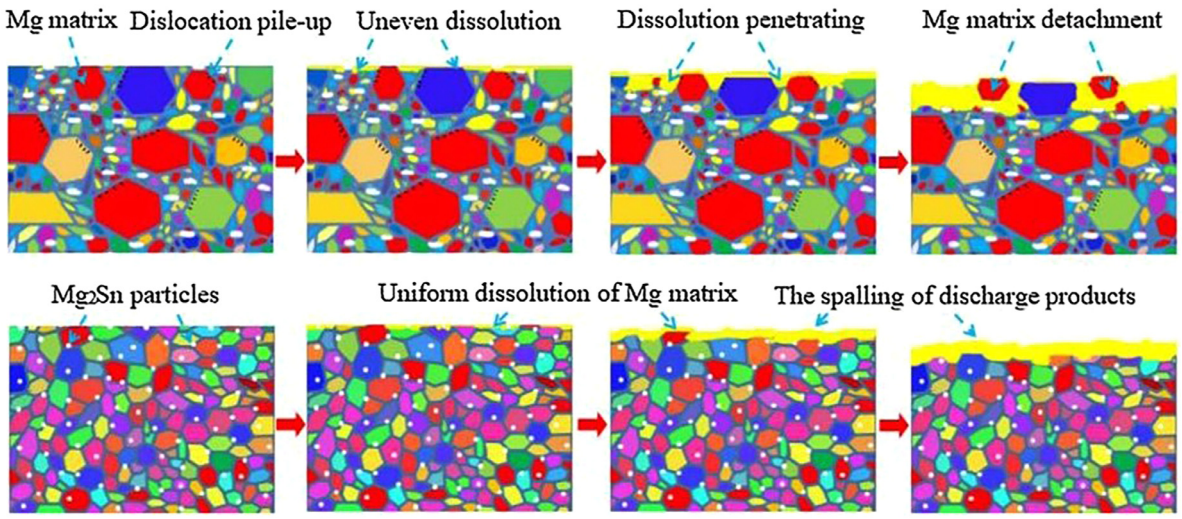

Fig. 12. Schematic illustration of the dissolution process of α-Mg matrix during discharge [67].

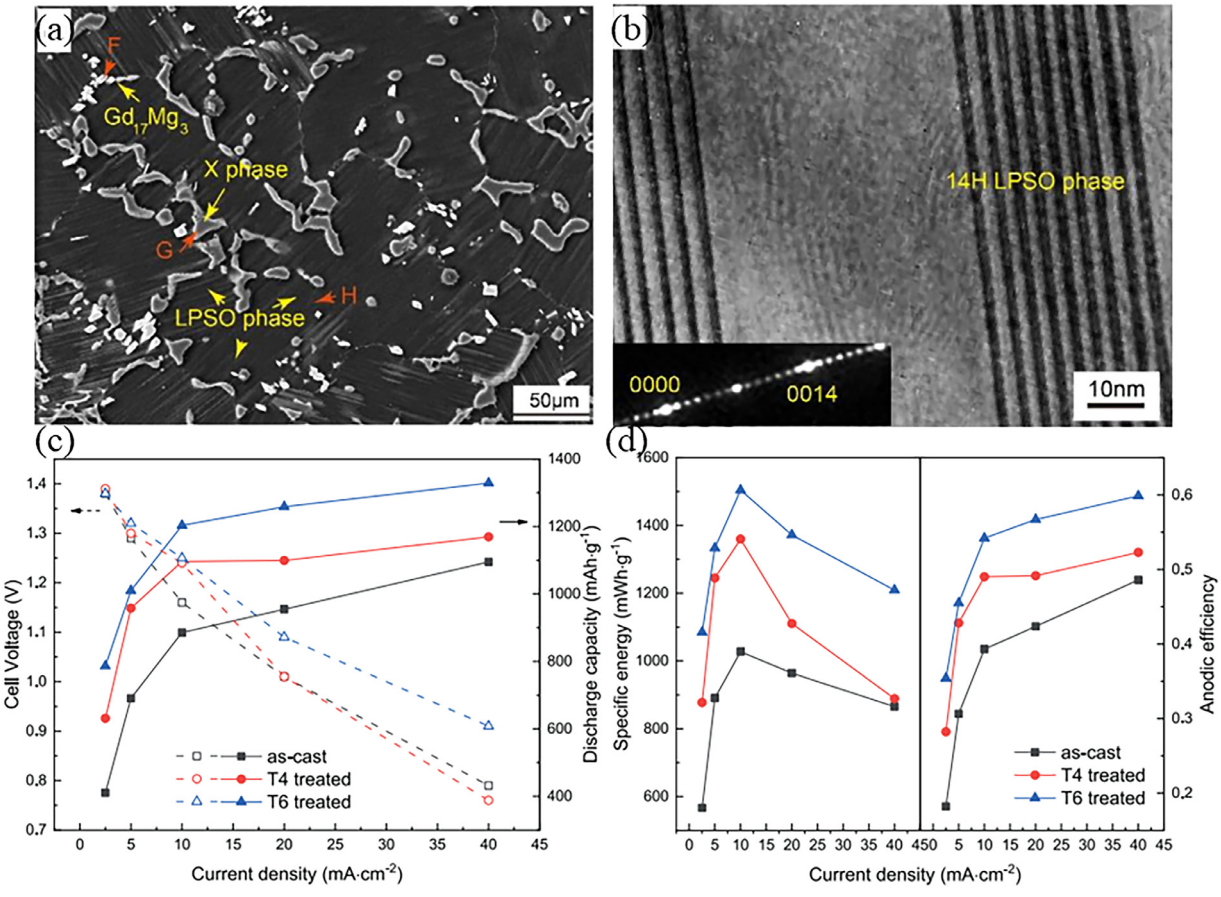

Fig. 13. (a) SEM image of T6 treated Mg-Gd-Zn, (b) TEM image of 14H LPSO phase, (c) discharge properties of cell voltage and discharge capacity, (d) discharge properties of anodic efficiency and specific energy. Reproduced with permission [159].

exposes fresh matrix, thus keeping discharge activity maintained [159,162]. Therefore, the LPSO phase can function as a phase that enhances corrosion resistance and discharge activity, ultimately introducing a new method for attaining high discharge capacity and anodic efficiency in MAB anodes.

4.2. Potential dendritic deposition for risk

It is generally believed that the dendrite-free growth and deposition behaviors of MAB is a safety feature that particularly superior to Li-based anode. This mature perspec-

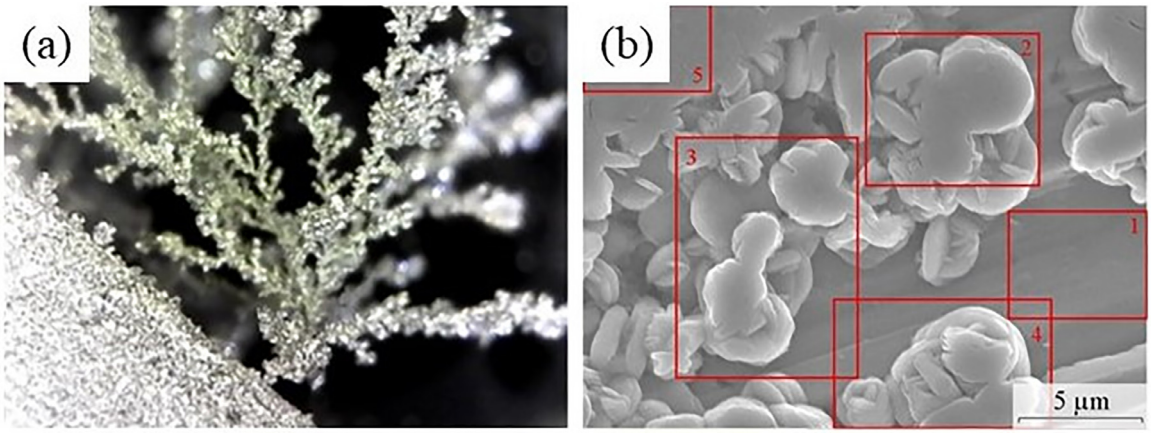

Fig. 14. Images of: (a) dendritic magnesium deposits. Reproduced with permission [165]. (b) Spherical dendritic magnesium deposits. Reproduced with permission [167].

tive originates from the theorization of the high self-diffusion rate, Ehrlich-Schwö-bel diffusion rate, and single-bonding strength of Mg. The tendency towards forming high dimensional crystalline layer during electrochemical deposition rather than dendrites [163,164]. Recent studies have challenged this perception. As the electrochemical reaction rate is considerably higher than the self-diffusion rate during the electroplating process, Mg also tends to deposit unevenly and produce dendritic deposits like Li, as shown in Fig. 14(a) [165]. This phenomenon can be associated with the influence of texture. The preferred growth direction of α-Mg dendrites is in the prismatic texture, which possesses high surface energy. In contrast, the basal texture surface does not have a propensity to deposit dendrites [164,166]. Consequently, the thermodynamic of the low surface energy basal texture tends to be stable at low current density or low electrodeposition rate, facilitating the rapid self-diffusion of Mg ions. It decreases the disparity in the electrochemical reaction rate and encourages consistent deposition of products.

An additional reason for the challenge in achieving uniform deposition resulting in dendrites is that Mg ions do not transit easily through the dense products layer of basal texture, and preferentially penetrate at the defect site of the products layer [4]. It further affects the dissolution and deposition of the discharged Mg anode, results in local high current density, accelerating electrochemical reactions and promoting dendrite growth. It is worth noting that this theory is based on the formation of a significant deposition layer after multiple discharge cycles of Mg anodes, rather than single discharge. Therefore, theories suggesting the dendrite-free behavior of Mg anodes after single discharge may be one-sided, especially since MAB has the potential for cyclic discharge. Based on the above discussion, the dendritic growth of Mg anodes is dependent on the current density and its impact on the electrochemical reaction rate. Kwak et al. [168] studied the critical current density by observing the dendrite growth process of the Mg anode. Meanwhile, certain studies have suggested that the electrolyte plays a crucial role in causing the dendritic fractal growth of Mg anode deposits [163,165]. Ding et al. [167] reported that the Mg anode deposits tend to form spherical dendritic deposits in $Mg(TFSI)_2$/glyme electrolyte, as shown in Fig. 14(b), which comprised of Mg, MgO, MgF_2, and MgS. Similar to the aforementioned factors, when Mg $(TFSI)_2$/glyme electrolyte is unable to fully corrode the surface of the Mg anode at certain concentrations, it creates areas of uneven discharge activity resulting in localized high current density, which ultimately leads to the formation of dendrites. Many evidences suggest that introducing magnesiopilics sites can effectively limit the rate of dendrite growth [168].

5. Discussion on the processing technology

The casting process aids in the development of the network structure of β-$Mg_{17}Al_{12}$ in Mg-Al anodes to hinder corrosion, reducing the effects of corrosion. It is commonly acknowledged that cast MAB anodes are prone to accumulation of discharge products on the active surface largely due to defects such as pores and impurities. Cast Mg anodes typically exhibit dendritic structures, leading to poor anodic efficiency and voltage instability. The impact of dendrites on the electrochemical behaviors of Mg anodes is more significant than that of textures, which required refinement [71,169]. On the other hand, the electrochemical activity of those produced via plastic deformation have excellent electrochemical activity with small grains and weaker textures [41–43]. Processing techniques such as plastic processing and heat treatment can enhance the electrochemical output of alloys by refining the organization uniformity, regulating grain size, and manipulating phase distribution.

5.1. Plastic deformation

In the previous discussion, it has been confirmed that Mg alloys produced via plastic deformation processes display exceptional electrochemical activity with refined grain and second phase sizes. Hot extrusion [170] and hot rolling [36,171]

aid in generating nano sub-grains throughout the matrix to enhance microstructure uniformity. Furthermore, the layer of products on these anode surfaces decomposed, leading to sustained the electrochemical activity. Compared to the as-cast Mg anode, the extruded Mg anode displays considerably fewer twins, dislocations, and other crystalline defects, resulting in a lessened occurrence of hydrogen evolution and chunk effect during the discharge [172]. Additionally, the rolling of the extruded Mg alloy sheet can further refine the grain and increase basal texture, resulting in a decrease in the self-corrosion rate. The improvement in anodic efficiency can be primarily attributed to the modification of grain size [74]. During the formation process, it is essential to consider the extrusion ratio and rolling reduction as significant parameters for impacting the performance of rolled Mg anodes [173]. Shangguan et al. [174] demonstrated the Mg-Bi-Ag-In anode, extruded with a ratio of 9, exhibited a bimodal microstructure consisting of equiaxed and elongated deformed grains. Comparatively, an extrusion ratio of 36, resulted in enhanced discharge performance attributed to the fine-equiaxed grain structure.

The process of plastic deformation manufacturing reduces grain size and enhance texture transformation. This, in turn, promotes the uniform dissolution of alloy constituents and the dissolution of large-sized phase particles, thus improving and uniform distribution of alloy elements, the corrosion resistance of Mg alloy anodes is improved. Acceleration of discharge product detachment also improves the discharge activity. Microcracks tend to form on the surface of samples with plastic deformation that ensure the greater electrochemical activity [24].

5.2. Heat treatment

Heat treatment modifies the discharge properties of Mg anodes by changing their microstructure, particularly in cast Mg alloys [42,175]. In cast Mg-Zn anodes, heat treatment is capable of significantly enhancing the (10–12) texture content of α-Mg. Moreover, after T6 heat treatment, leads to the anode possessing a notably reactive discharge surface composed primarily of (10–11) and (01–10) textures. By the Mg_7Zn_3 eutectic phase dissolving, the micro-galvanic effect weakens and thus, the corrosion resistance improves [176]. Additionally, in the case of as-extruded Mg-Zn-Mn-Nd anodes, heat and subsequent aged treatment enhance the growth of the T_2 phase, which contains the $MgZn_2$ with $Mg_{52}Zn_{40}Nd_8$ phase. This might improve anodic efficiency at fine structure [177]. In the case of hot-rolled AP65 anodes, subsequent hot treatment reduces dislocation density effectively. However, at temperature of 350 °C, the equiaxed grains experience growth. Despite the size still being smaller than that of the as-cast alloy, the anodic efficiency drops significantly when compared to the 150 °C hot treatment [36]. Han et al. [178] were the first reported on the as-extruded Mg-4Li-3Nd-0.2Zn anode used in air batteries, with 450 °C heat treatment leading to lower volume fractions of the $Mg_{41}Nd_5$ phase and the anodic effiency increased from 31.29% to 48.37%. Xiong et al. [179] effectively promoted the uniform distribution and recrystallization of fine spherical Mg_2Sn phases in hot extruded Mg-6Al-1Sn though heat treatment at 200 °C, resulting in a uniform microstructure and improved discharge performance. Xiong et al. [42] also found that while heat treatment can improve the energy density of Mg-Al-Sn MAB anode, it does not enhance its capacity or anodic efficiency during discharge. The self-corrosion mainly caused by micro-galvanic corrosion aggravated by Sn with high potential. In addition, the phase transformation and twinning structure of magnesium alloy alloys are determined by the heat treatment temperature. For instance, the Mg-Li-Al alloy tends to occur $\beta \rightarrow \beta + \theta + \alpha$ at room temperature. While the transformation of $\beta \rightarrow \beta + \theta + \alpha +$ AlLi at 473 K [180]. The rolled AZ31B exhibits different microstructures with/without twinning at different heat treatment temperatures [57]. Additionally, the heat treatment parameters, particularly the temperature and duration of treatment significantly influence the grain size changes. Hence, these parameters necessitate careful consideration [178].

A variety of advanced forming technologies hold promise as processes for producing MAB anodes. These include magnetron-sputtering [181], spark plasma sintering [62], and microwave-assisted smelting, etc. [182]. For cast Mg anodes, segregation behavior of solutes in cast alloys and precipitation of chemical components can be promoted by homogenization treatment, in addition to hot treatment [63,158]. In conclusion, the objectives of these methods are to achieve superior microstructures, weaker texture strength and fewer defects, as shown in Fig. 15.

6. Electrically rechargeable MAB anode?

Mg anodes have demonstrated efficient cycling in numerous electrolyte systems [184], and have the potential for achieving rechargeable performance in air batteries. Currently, MAB primarily focuses on primary battery research. Researchers are pursuing the influential project of developing secondary MABs with cyclic discharge for achieving high discharge capacity and anodic efficiency. On one hand, the process of charging and discharging necessitates the substitution of mechanically rechargeable fresh electrodes after the anodic discharge cycle (mechanically). Or the direct implementation of rechargeable MAB anode (electrically). Although the Mg anode have the potential used for rechargeable MAB, it is still hard to achieve the electrically rechargeable [13,185]. As the assumption of the electrically rechargeable Mg anode, this section offers guidance to researchers on developing design methodologies based on the microstructural features of the anode.

In previous discussions, the factors limiting the cyclic discharge performance of MAB have been identified as slow kinetics, unstable discharge voltage, attenuated anodic efficiency, and potential dendrite risk during cycling. To achieve stable cycling, many forming processes and alloying strategies aim to form uniform microstructures that increase specific active area and reduce ion diffusion losses. These techniques are vital in achieving stable cycling. Currently, the focus of

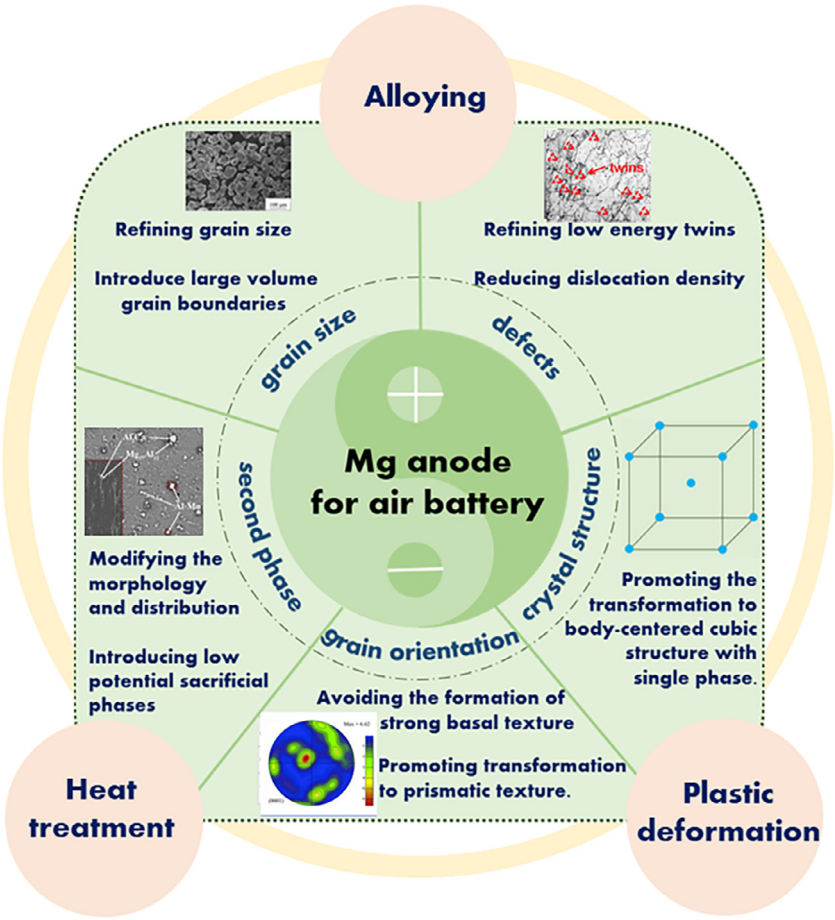

Fig. 15. Schematic showing the design and optimization methods of Mg anode used for air battery. Reproduced with permissions [62,124,154,183].

research is on developing mixed electrolytes, efficient cathode catalysts, and cathode material modifications, with the aim of forming MgO_2 and MgO products reversibly. Zhang et al. [13] argued that MgO_2 has greater electrochemical potential than MgO. In order to facilitate comprehension of the defects in the anode of MAB, it is imperative to suppress the attachment of discharge products to the surface to ensure contact between the matrix and electrolyte. One way of achieving this is through the creation of a tailored structure, for example, a layered LPSO phase, which encourages the self-peeling of discharge products and thereby sustains its effectiveness. The corrosion resistance is related to the loss of undischarged anode quality and achieved anodic efficiency. In Mg alloys with poor corrosion resistance the deposition layer is relied upon. However, the detachment of the deposition layer necessitates improving corrosion resistance though internal microstructure. This entails lowering the potential of second phases through alloying, which weakens the microgalvanic effect. Although the consistent dissolution state of the matrix may be the reason for the contradiction of texture influence, research on the cycling performance of MAB with different grain orientations anodes is limited. It can be inferred that the better choice is the uniformly dissolved prismatic texture with high anodic efficiency and active discharge performance. However, the preferential growth of twins, dislocations, and even dendrite deposition caused by prismatic texture has not been confirmed. Similarly, additional factors to consider are grain size. The NDE can readily produce pressure imbalances in the MAB system. By refining the grains and introducing grain boundaries in the Mg anode, damage caused by the NDE can be minimized. Liang et al. [186] have explored the use of nanoscale Mg particles for the anode of rechargeable Mg batteries. This anode has a high reversible discharge capacity, making it a good the candidate for MAB. In addition, the selection of appropriate electrolytes plays a crucial role in dendrite growth potential. Reasonably designing voltage/current thresholds to suppress dendrite growth and ensure the safety of the MAB during cycling.

7. Summary and outlook

As a new generation of clean energy, MAB effectively achieves renewable utilization of resources while reducing carbon emissions. Obtaining Mg anode with high discharge activity and anodic efficiency has always been the design vision of researchers. Based on the literature analysis, the relationship between the microstructure of Mg alloy and the discharge performance of MAB is still a major research hotspot. Although an amount of work has promoted the development

of MAB, there is almost no examination of anodes at the topic.

In fact, the main method of improving the discharge performance of Mg alloy anode materials is regulating the microstructure characteristics. Therefore, this work examined and developed strategies for advance MAB anodes from the perspective of the microstructure. The discussion also includes the poor corrosion resistance and NDE characteristics of Mg alloys, as well as the evolution of microstructure during forming and modification. Hereto, we have summarized as follows:

(1) Small grain size, low density twinning and dislocations, second phase of specific shape, and introduction of LPSO phase are the strategies to enhance the discharge performance of MAB.
(2) Poor corrosion resistance and the derived NDE have always limited the application of MAB. While ensuring smooth detachment of the products layer is prone to maintain electrochemical activity, weakening the microgalvanic effect is the key to corrosion prevention.
(3) Contrary to corrosion behavior, the prismatic discharge surface is superior to the basal discharge because of the uniform dissolution with less chunk effect.
(4) Suitably plastic deformation and heat treatment are key means to achieve ideal microstructure and improve anode efficiency of MAB.
(5) In addition to the selection of electrolytes and catalyzers, the microstructure of Mg anode is also the key to the design of MAB.

At present, the application of magnesium alloy as anode material for air batteries is still in the early stage, and the discharge performance of batteries still has great room for improvement. The future research can be carried out from the following aspects: (1) further control of the microstructure, such as the grain size of micro-nano structure, small uniform and dispersed second phase, grain surface with prismatic texture, etc. (2) Given that various microstructures may not synergistically evolve towards ideal design, machine learning can be a new method to find out the dominance among the microstructures, and obtain the optimum MAB anode; (3) The single crystal Mg anode with prismatic texture may the ideal MAB anode due to the high electrochemical activity and weaken “chunk effect”.

Declaration of competing interest

The author declares that he has no known competing financial interests or personal relationships that could have appeared to influence the work reported in this paper.

CRediT authorship contribution statement

Xu Huang: Conceptualization, Data curation, Methodology, Writing – original draft. **Qingwei Dai:** Formal analysis, Project administration, Resources, Writing – original draft, Funding acquisition. **Qing Xiang:** Data curation, Resources, Writing – original draft. **Na Yang:** Writing – review & editing. **Gaopeng Zhang:** Writing – review & editing. **Ao Shen:** Writing – review & editing. **Wanming Li:** Methodology.

Acknowledgement

The work is supported by National Natural Science Foundation of China (52371095), Innovation Research Group of Universities in Chongqing (CXQT21030), Chongqing Talents: Exceptional Young Talents Project (CQYC201905100), Chongqing Youth Expert Studio, Chongqing Overseas Chinese Entrepreneurship and Innovation Support Program (cx2023117), Chongqing Natural Science Foundation Innovation and Development Joint Fund (CSTB 2022NS CQ-LZX0054).

References

[1] G. Crabtree, Science 366 (6464) (2019) 422–424, doi:10.1126/science.aax0704.
[2] L. Grande, E. Paillard, J. Hassoun, J.B. Park, Y.J. Le, Y.K. Sun, S. Passerini, B. Scrosati, Adv. Mater. 27 (5) (2015) 784–800, doi:10.1002/adma.201403064.
[3] A. Suryatna, I. Raya, L. Thangavelu, F.R. Alhachami, M.M. Kadhim, U.S. Altimari, Z.H. Mahmoud, Y.F. Mustafa, E. Kianfar, J. Chem NY. 2022 (2022) 2762647, doi:10.1155/2022/2762647.
[4] F.F. Liu, G.Q. Cao, J.J. Ban, H.H. Lei, Y. Zhang, G.S. Shao, A.G. Zhou, L.Z. Fan, J.H. Hu, J. Magnes. Alloy. 10 (10) (2022) 2699–2716, doi:10.1016/j.jma.2022.09.004.
[5] X.X. Zhang, L. Li, E.S. Fan, Q. Xue, Y.F. Bian, F. Wu, R.J. Chen, Chem. Soc Rev. 47 (19) (2018) 7239–7302, doi:10.1039/C8CS00297E.
[6] G. Kuang, H. Li, S. Hu, R. Jin, S.J. Liu, H. Guo, Hydrometallurgy 157 (2015) 214–218, doi:10.1016/j.hydromet.2015.08.020.
[7] M. Salado, E. Lizundia, Mater. Today. Energy. 28 (2022) 101064, doi:10.1016/j.mtener.2022.101064.
[8] N. Chawla, Mater. Today. Chem. 12 (2019) 324–331, doi:10.1016/j.mtchem.2019.03.006.
[9] Y.E. Durmus, H. Zhang, F. Baakes, G. Desmaizieres, H. Hayun, L. Yang, M. Kolek, V. Küpers, J. Janek, D. Mandler, S. Passerini, Y. Ein-Eli, Adv. Energy. Mater. 10 (24) (2020) 2000089, doi:10.1002/aenm.202000089.
[10] J. Xu, Z.N. Wei, L.C. Tang, A. Wang, Y. Zhang, Y.H. Qiao, C.G. Chen, J. Power. Sources. 454 (2020) 227869, doi:10.1016/j.jpowsour.2020.227869.
[11] J.L. Ma, Y. Zhang, M.S. Ma, C.H. Qin, F.Z. Ren, G.X. Wang, Corros. Sci. 170 (2020) 108695, doi:10.1016/j.corsci.2020.108695.
[12] C.S. Li, Y. Sun, F. Gebert, S.L. Chou, Adv. Energy. Mater. 7 (24) (2017) 1700869, doi:10.1002/aenm.201700869.
[13] T.R. Zhang, Z.L. Tao, J. Chen, Mater. Horiz. 1 (2) (2014) 196–206, doi:10.1039/C3MH00059A.
[14] L. Zhang, Q.S. Shao, J.J. Zhang, Reports: Energy 1 (1) (2021) 100002, doi:10.1016/j.matre.2020.11.001.
[15] N.G. Wang, R.C. Wang, C.Q. Peng, C.W. Hu, F. Yan, B. Peng, T. Nonferr. Metal. Soc. 24 (8) (2014) 2427–2439, doi:10.1016/S1003-6326(14)63367-7.
[16] M. Arsentev, A. Missyul, A.V. Petrov, M. Hammouri, J. Phys. Chem. C. 121 (29) (2017) 15509–15515, doi:10.1021/acs.jpcc.7b01575.
[17] C.M. MacLaughlin, ACS. Energy. Lett. 4 (2) (2019) 572–575, doi:10.1021/acsenergylett.9b00214.
[18] W. Sun, F. Wang, B. Zhang, M.Y. Zhang, V. Küpers, X. Ji, C. Theile, P. Bieker, K. Xu, C.S. Wang, M. Winter, Science 371 (6524) (2021) 46–51, doi:10.1126/science.abb9554.
[19] F. Santos, A. Urbina, J. Abad, R. López, C. Toledo, A.J. Fernández Romero, Chemosphere 250 (2020) 126273, doi:10.1016/j.chemosphere.2020.126273.

[20] Q. Sun, H. Yadegari, M.N. Banis, J. Liu, B. Xiao, X. Li, C. Langford, R.Y. Li, X.L. Sun, J. Phys. Chem. C. 119 (24) (2015) 13433–13441, doi:10.1021/acs.jpcc.5b02673.
[21] W.W. Yin, Z.W. Fu, ChemCatChem 9 (9) (2017) 1545–1553, doi:10.1002/cctc.201600646.
[22] M.A. Deyab, Q. Mohsen, Renew. Sust. Energ. Rev. 139 (2021) 110729, doi:10.1016/j.rser.2021.110729.
[23] W.K. Tan, K. Asami, Y. Maeda, K. Hayashi, G. Kawamura, H. Muto, A. Matsuda, Appl. Surf. Sci. 486 (2019) 257–264, doi:10.1016/j.apsusc.2019.04.278.
[24] F.L. Tong, S.H. Wei, X.Z. Chen, W. Gao, J. Magnes. Alloy. 9 (6) (2021) 1861–1883, doi:10.1016/j.jma.2021.04.011.
[25] X.R. Chen, Y.H. Jia, Z.M. Shi, Q.C. Le, J.R. Li, M.X. Zhang, M. Liu, A. Atrens, J. Mater. Chem. A. 9 (37) (2021) 21387–21401 2021, doi:10.1039/D1TA04320J.
[26] G. Song, A. Atrens, Adv. Eng. Mater. 5 (12) (2003) 837–858, doi:10.1002/adem.200310405.
[27] Y.C. Zhao, G.S. Huang, G.G. Wang, T.Z. Han, F.S. Pan, Acta. Metall. Sin. 28 (011) (2015) 1387–1393, doi:10.1007/s40195-015-0337-2.
[28] S. Bender, J. Goellner, A. Heyn, S. Schmigalla, Mater. Corros. 63 (8) (2012) 707–712, doi:10.1002/maco.201106225.
[29] T.R. Thomaz, C.R. Weber, T. Pelegrini Jr, L.F.P. Dick, G. Knörnschild, Corros. Sci. 52 (7) (2010) 2235–2243, doi:10.1016/j.corsci.2010.03.010.
[30] W.T. Zhang, Q.J. Liu, Y.Q. Chen, G.J. Wan, Mater. Lett. 232 (2018) 54–57, doi:10.1016/j.matlet.2018.08.069.
[31] G.S. Frankel, A. Samaniego, N. Birbilis, Corros. Sci. 70 (2013) 104–111, doi:10.1016/j.corsci.2013.01.017.
[32] G. Song, Adv. Eng. Mater. 7 (7) (2005) 563–586, doi:10.1002/adem.200500013.
[33] A. Atrens, W. Dietzel, Adv. Eng. Mater. 9 (4) (2007) 292–297, doi:10.1002/adem.200600275.
[34] Z.M. Shi, J.X.S. Jia, A. Atrens, Corros. Sci. 60 (2012) 296–308, doi:10.1016/j.corsci.2011.12.002.
[35] J. Huang, G.L. Song, A. Atrens, M. Dargusch, J. Mate. Sci. Technol. 57 (2020) 204–220, doi:10.1016/j.jmst.2020.03.060.
[36] N.G. Wang, R.C. Wang, C.Q. Peng, Y. Feng, B. Chen, Corros. Sci. 64 (2012) 17–27, doi:10.1016/j.corsci.2012.06.024.
[37] L.H. Li, H. Chen, E. He, L. Wang, T.T. Ye, J. Lu, Y.D. Jiao, J.C. Wang, R. Gao, H.S. Peng, Y. Zhang, Angew, Chem. Int. Edit. 60 (28) (2021) 15317–15322, doi:10.1002/ange.202104536.
[38] M. Deng, L.Q. Wang, B. Vaghefinazari, W. Xu, C. Feiler, S.V. Lamaka, D. Höche, M.L. Zheludkevich, D. Snihirova, Energy. Storage. Mater. 43 (2021) 238–247, doi:10.1016/j.ensm.2021.09.008.
[39] L.D. Chen, J.K. Nørskov, A.C. Luntz, J. Phys. Chem. C. 119 (34) (2015) 19660–19667, doi:10.1021/acs.jpcc.5b05677.
[40] M. Deng, D. Höche, S.V. Lamaka, D. Snihirova, M.L. Zheludkevich, J. Power. Sources. 396 (2018) 109–118, doi:10.1016/j.jpowsour.2018.05.090.
[41] T.X. Zheng, Y.B. Hu, S.W. Yang, J. Magnes. Alloy. 5 (4) (2017) 404–411, doi:10.1016/j.jma.2017.09.003.
[42] H.Q. Xiong, H.L. Zhu, J. Luo, K. Yu, C.L. Shi, H.J. Fang, Y. Zhang, J. Mater. Eng. Perform. 26 (6) (2017) 1–11, doi:10.1007/s11665-017-2733-4.
[43] Y.P. Wu, Z.F. Wang, Y. Liu, G.F. Li, S.H. Xie, H. Yu, H.Q. Xiong, J. Mater. Eng. Perform. 28 (4) (2019) 2006–2016, doi:10.1007/s11665-019-03985-5.
[44] X.R. Chen, Q. Zou, Q.C. Le, J. Hou, R.Z. Guo, H.N. Wang, C.L. Hu, L. Bao, T. Wang, D.Z. Zhao, F.X. Yu, A. Atrens, J. Power. Sources. 451 (2020) 227807, doi:10.1016/j.jpowsour.2020.227807.
[45] M. Yuasa, X. Huang, K. Suzuki, M. Mabuchi, Y. Chino, J. Power. Sources. 297 (2015) 449–456, doi:10.1016/j.jpowsour.2015.08.042.
[46] F.L. Tong, X.R. Chen, S.H. Wei, J. Malmström, J. Vella, W. Gao, J. Magnes. Alloy. 9 (6) (2021) 1967–1976, doi:10.1016/j.jma.2021.08.022.
[47] X.R. Chen, Q. Zou, Z.M. Shi, Q.C. Le, M.X. Zhang, A. Atrens, Electrochim. Acta. 404 (2022) 139763, doi:10.1016/j.electacta.2021.139763.
[48] G.L. Song, Z.Q. Xu, Corros. Sci. 54 (2012) 97–105, doi:10.1016/j.corsci.2011.09.005.
[49] C.J. Yan, Y.C. Xin, X.B. Chen, D.K. Xu, P.K. Chu, C.Q. Liu, B. Guan, X. Huang, Q. Liu, Nat. Commun. 12 (1) (2021) 4616, doi:10.1038/s41467-021-24939-3.
[50] A. Schreiber, C. Rosenkranz, M.M. Lohrengel, Electrochim. Acta. 52 (27) (2007) 7738–7745, doi:10.1016/j.electacta.2006.12.062.
[51] C.op't. Hoog, N. Birbilis, Y. Estrin, Adv. Eng. Mater. 10 (6) (2008) 579–582, doi:10.1002/adem.200800046.
[52] C.X. Duan, J.G. Tang, W.J. Ma, L.Y. Ye, H.C. Jiang, Y.L. Deng, X.M. Zhang, J Mater. Sci. 55 (2020) 10833–10848, doi:10.1007/s10853-020-04692-6.
[53] V. Guillaumin, G. Mankowski, Corros. Sci. 42 (1) (2000) 105–125, doi:10.1016/S0010-938X(99)00053-0.
[54] M.Y. Chen, Y.L. Deng, J.G. Tang, S.T. Fan, X.M. Zhang, Mater. Charact. 148 (2019) 259–265, doi:10.1016/j.matchar.2018.12.024.
[55] J.W. Li, Y.M. Qiu, J.J. Yang, Y.Y. Sheng, Y.L. Yi, X. Zeng, L.X. Chen, F.L. Yin, J.Z. Su, T.J. Zhang, X. Tong, B. Guo, J. Magnes. Alloy. 11 (1) (2023) 217–229, doi:10.1016/j.jma.2021.04.007.
[56] J.S. Liao, M. Hotta, N. Yamamoto, Corros.Sci 61 (2012) 208–214, doi:10.1016/j.corsci.2012.04.039.
[57] N.N. Aung, Z. Wei, Corros. Sci. 52 (2) (2010) 589–594, doi:10.1016/j.corsci.2009.10.018.
[58] G.R. Argade, S.K. Panigrahi, R.S. Mishra, Corros. Sci. 58 (5) (2012) 145–151, doi:10.1016/j.corsci.2012.01.021.
[59] K.D. Ralston, N. Birbilis, Corrosion 66 (2010) 1–4, doi:10.5006/1.3462912.
[60] H.B. Yang, L. Wu, B. Jiang, W. Liu, J.F. Song, G.S. Huang, D.F. Zhang, F.S. Pan, J. Mater. Sci. Technol. 62 (2021) 128–138, doi:10.1016/j.jmst.2020.05.067.
[61] A.R. Eivani, M. Mehdizade, S. Chabok, J. Zhou, J. Mater. Res. Technol. 12 (2021) 1946–1957, doi:10.1016/j.jmrt.2021.03.021.
[62] N.G. Wang, Y.X. Huang, J.J. Liu, X.S. Yang, W.P. Xie, Q. Cai, S.Y. Zheng, Z. Shi, Electrochim. Acta. 378 (2021) 138135, doi:10.1016/j.electacta.2021.138135.
[63] N.G. Wang, R.C. Wang, C.Q. Peng, B. Peng, Y. Feng, C.W. Hu, Electrochim. Acta. 149 (2014) 193–205, doi:10.1016/j.electacta.2014.10.053.
[64] Y. Feng, W.H. Xiong, J.C. Zhang, R.C. Wang, N.G. Wang, J. Mater. Chem. A. 4 (22) (2016) 8658–8668, doi:10.1039/C6TA02574A.
[65] S. Linjee, S. Moonngam, P. Klomjit, N.S. Pålsson, C. Banjongprasert, Energy. Rep. 8 (2022) 5117–5128, doi:10.1016/j.egyr.2022.03.132.
[66] X.B. Zheng, T. Zhang, H.J. Yang, Q.L. Zheng, Y.M. Gao, Z.W. Liu, W. Wang, K.S. Wang, Electrochim. Acta. 354 (10) (2020) 163365, doi:10.1016/j.electacta.2020.136635.
[67] X.J. Gu, W.L. Cheng, S.M. Cheng, Y.H. Liu, Z.F. Wang, H. Yu, Z.Q. Cui, L.F. Wang, H.X. Wang, J. Mater. Sci. Technol. 60 (2021) 77–89, doi:10.1016/j.jmst.2020.04.057.
[68] X.R. Chen, S.C. Ning, Q.C. Le, H.N. Wang, Q. Zou, R.Z. Guo, J. Hou, Y.H. Jia, A. Atrens, F.X. Yu, J. Mater. Sci. Technol. 38 (2020) 47–55, doi:10.1016/j.jmst.2019.07.043.
[69] Y.H. Chen, W.L. Cheng, X.J. Gu, H. Yu, H.X. Wang, X.F. Niu, L.F. Wang, H. Li, J. Alloy. Compd. 886 (2021) 161271, doi:10.1016/j.jallcom.2021.161271.
[70] S.M. Cheng, W.L. Cheng, X.J. Gu, H. Yu, Z.F. Wang, H.X. Wang, L.F. Wang, J. Alloy. Compd. 823 (2020) 153779, doi:10.1016/j.jallcom.2020.153779.
[71] X.R. Chen, Q.Y. Liao, Q.C. Le, Q. Zou, H.N. Wang, A. Atrens, Electrochim. Acta. 348 (2020) 136315, doi:10.1016/j.electacta.2020.136315.
[72] S.Y. Wang, J.Q. Wang, Corros. Sci. 85 (2014) 183–192, doi:10.1016/j.corsci.2014.04.014.
[73] G.L. Song, Z.Q. Xu, Corros. Sci. 63 (2012) 100–112, doi:10.1016/j.corsci.2012.05.019.
[74] B. Jiang, Q. Xiang, A. Atrens, J.F. Song, F.S. Pan, Corros. Sci. 126 (2017) 374–380, doi:10.1016/j.corsci.2017.08.004.
[75] A. Bahmani, S. Arthanari, K.S. Shin, J. Magnes. Alloy. 8 (1) (2020) 134–149, doi:10.1016/j.jma.2019.12.001.

[76] J.M. Song, Y.S. Zou, C.C. Kuo, S.C. Lin, Corros. Sci. 74 (2013) 223–231, doi:10.1016/j.corsci.2013.04.046.
[77] E. Martinez-Lombardia, Y. Gonzalez-Garcia, L. Lapeire, I.D. Graeve, K. Verbeken, L. Kestens, J.M.C. Mol, H. Terryn, Electrochim. Acta. 116 (2014) 89–96, doi:10.1016/j.electacta.2013.11.048.
[78] J.M. Ren, J.B. Ma, J. Zhang, C.P. Fu, B.D. Sun, J. Alloy. Compd. 808 (2019) 151708, doi:10.1016/j.jallcom.2019.151708.
[79] M. Liu, D. Qiu, M.C. Zhao, G.L. Song, A. Atrens, Scripta. Mater. 58 (5) (2008) 421–424, doi:10.1016/j.scriptamat.2007.10.027.
[80] T. Mandai, H. Somekawa, Chem. Commun. 56 (81) (2020) 12122–12125, doi:10.1039/D0CC05373B.
[81] H.B. Yang, L. Bin, L. Wu, B. Jiang, W.J. Liu, Q. Yang, J.F. Song, G.S. Huang, D.F. Zhang, F.S. Pan, J. Electrochem. Soc. 167 (13) (2020) 130528, doi:10.1149/1945-7111/abbb0b.
[82] W.L. Cheng, Y.J. Chen, X.J. Gu, J. Feng, H. Yu, H.X. Wang, X.F. Niu, L.F. Wang, H. Li, J. Power. Sources. 520 (2022) 230802, doi:10.1016/j.jpowsour.2021.230802.
[83] N.G. Wang, Y.C. Mu, W.H. Xiong, J.C. Zhang, Q. Li, Z.C. Shi, Corros. Sci. 144 (2018) 107–126, doi:10.1016/j.corsci.2018.08.003.
[84] H.B. Yang, L. Wu, B. Jiang, B. Lei, M. Yuan, H.M. Xie, A. Atrens, J.F. Song, G.S. Huang, F.S. Pan, Int. J. Min. Met. Maters. 28 (10) (2021) 1705–1715, doi:10.1007/s12613-021-2258-6.
[85] H.A. Robinson, Trans. Electrochem 90 (1) (1946) 485, doi:10.1149/1.3071762.
[86] I. Nakatsugawa, Y. Chino, Mater. Trans. 61 (1) (2020) 200–205, doi:10.2320/matertrans.MT-M2019259.
[87] Y.C. Zhao, G.S. Huang, C. Zhang, L. Chen, T.Z. Han, F.S. Pan, Rar. Metal. Mater. En. 47 (4) (2018) 1064–1068, doi:10.1016/S1875-5372(18)30121-8.
[88] C.W. Gong, X.Z. He, D.P. Fang, B.S. Liu, X. Yan, J. Alloy. Compd. 861 (2021) 158493, doi:10.1016/j.jallcom.2020.158493.
[89] Y.M. Jin, C. Blawert, F. Feyerabend, J. Bohlen, M.S. Campos, S. Gavras, B. Wiese, D. Mei, M. Deng, H. Yang, R. Willumeit-Römer, Corros. Sci. 158 (2019) 108096, doi:10.1016/j.corsci.2019.108096.
[90] L.B. Wang, P.J. Li, L.J. He, Russ. J. Electrochem. 47 (8) (2011) 900–907, doi:10.1134/S1023193511080167.
[91] B. Xiao, F.Y. Cao, T. Ying, Z.M. Wang, D.J. Zheng, W.C. Zhang, G.L. Song, ACS. Appl. Mater. Interfaces. 13 (49) (2021) 58737–58745, doi:10.1021/acsami.1c18913.
[92] H. Liu, Y. Yan, X.H. Wu, H.J. Fang, X. Chu, J.F. Huang, J.X. Zhang, J.M. Song, K. Yu, J. Alloy. Compd. 859 (2021) 157755, doi:10.1016/j.jallcom.2020.157755.
[93] J.X. Bao, L.H. Li, J.C. Sha, M.L. Qiao, J. Tian, W.H. Liu, Z.Q. Zhang, Electrochim. Acta. 465 (2023) 143014, doi:10.1016/j.electacta.2023.143014.
[94] F.L. Tong, X.Z. Chen, T.E. Teoh, S.H. Wei, G.I.N. Waterhouse, W. Gao, J. Electrochem. Soc. 168 (11) (2021) 110531, doi:10.1149/1945-7111/ac3716.
[95] Z.H. Chen, Y.A. Zhang, M.L. Ma, K. Zhang, Y.J. Li, G.L. Shi, J.W. Yuan, Z.Q. Sun, G. Zhao, Mater. Chem. Phys. 300 (1) (2023) 127500, doi:10.1016/j.matchemphys.2023.127500.
[96] J.X. Bao, J.C. Sha, L.H. Li, Z.L. Liu, J. Tian, W.H. Liu, J.Z. Cui, Z.Q. Zhang, J. Alloy. Compd. 934 (2023) 167849, doi:10.1016/j.jallcom.2022.167849.
[97] T.H. Le, P.L. Mao, W.Y. Hu, Q.C. Le, J. Electrochem. Soc. 170 (9) (2023) 090522, doi:10.1149/1945-7111/acf247.
[98] N. Shrestha, K.S. Raja, V. Utgikar, J. Electrochem. Soc. 166 (14) (2019) A3139, doi:10.1149/2.0131914jes.
[99] N. Shrestha, J. Zillinger, V. Utgikar, K.S. Raja, ECS. Trans. 85 (13) (2018) 95, doi:10.1149/08513.0095ecst.
[100] B.J. Ma, C. Tan, L.Z. Ouyang, H.Y. Shao, N.G. Wang, M. Zhu, J. Alloy. Compd. 918 (2022) 165803, doi:10.1016/j.jallcom.2022.165803.
[101] X.R. Chen, J. Venezuela, M. Dargusch, Electrochim. Acta. 448 (2023) 142127, doi:10.1016/j.electacta.2023.142127.
[102] Y.Z. Lv, M. Liu, Y. Xu, D.X. Cao, J. Feng, R.Z. Wu, M.L. Zhang, J. Power. Sources. 239 (2013) 265–268, doi:10.1016/j.jpowsour.2013.03.112.
[103] F.L. Tong, X.Z. Chen, Q. Wang, S.H. Wei, W. Gao, J. Alloy. Compd. 857 (2021) 157579, doi:10.1016/j.jallcom.2020.157579.
[104] Y.F. Song, J.L. Ma, Y.Q. Li, G.X. Wang, C.H. Qin, H.R. Stock, Ionics 25 (12) (2019) 5899–5906, doi:10.1007/s11581-019-03144-9.
[105] B. Xiao, G.L. Song, D.J. Zheng, Mater. Design 194 (2020) 108931, doi:10.1016/j.matdes.2020.108931.
[106] J.L. Ma, G.X. Wang, Y.Q. Li, F.Z. Ren, A.A. Volinsky, Ionics 25 (5) (2019) 2201–2209, doi:10.1007/s11581-018-2705-1.
[107] Z.Y. Li, H.X. Wang, J.J. Li, Y.P. Zhuang, J.Z. Gao, H. Li, W.L. Cheng, Adv. Eng. Mater. 22 (3) (2020) 1901332, doi:10.1002/adem.201901332.
[108] H.N. Wang, X.R. Chen, Q.C. Le, Q. Zou, Mater. Res. Express. 8 (4) (2021) 046521, doi:10.1088/2053-1591/abf285.
[109] T.X. Zheng, Y.B. Hu, Y.X. Zhang, S.W. Yang, Mater. Design. 137 (2018) 245–255, doi:10.1016/j.matdes.2017.10.031.
[110] I. Nakatsugawa, Y. Chino, J. Electrochem. Soc. 168 (5) (2021) 050507, doi:10.1149/1945-7111/abfb33.
[111] Q. Zou, Q.C. Le, Y.H. Jia, X.R. Chen, C.Y. Ban, H.N. Wang, Z.Y. Yin, L. Ren, T. Wang, Y.J. Zhang, Int. J. Energ. Res. 12 (46) (2022) 16870–16882, doi:10.1002/er.8354.
[112] N.G. Wang, R.C. Wang, C.Q. Peng, Y. Feng, X.Y. Zhang, T. Nonferr. Metal. Soc. 20 (8) (2010) 1403–1411, doi:10.1016/S1003-6326(09)60312-5.
[113] X.D. Li, H.M. Lu, S.Q. Yuan, J.J. Bai, J.R. Wang, Y. Cao, Q.S. Hong, J. Electrochem. Soc. 164 (13) (2017) A3131, doi:10.1149/2.0971713jes.
[114] M. Deng, L.Q. Wang, D. Höche, S.V. Lamaka, P.L. Jiang, D. Snihirova, N. Scharnagl, M.L. Zheludkevich, J. Power. Sources. 472 (2020) 228528, doi:10.1016/j.jpowsour.2020.228528.
[115] Y. Feng, G. Lei, Y.Q. He, R.C. Wang, X.F. Wang, T. Nonferr. Metal. Soc. 28 (11) (2018) 2274–2286, doi:10.1016/S1003-6326(18)64872-1.
[116] Y.Q. Li, J.L. Ma, G.X. Wang, F.Z. Ren, Y.J. Zhu, Y.F. Song, J.L. Zhang, Mater. Res. Express. 6 (6) (2019) 066315, doi:10.1088/2053-1591/ab0fb6.
[117] Q. Li, W. Xiong, M.H. Yu, J. Li, L. Liu, G. Zhu, L.Y. Wang, J. Wang, S.R. Yu, E.Y. Liu, J. Alloy. Compd. 891 (2022) 161914, doi:10.1016/j.jallcom.2021.161914.
[118] H.L. Zhu, H. Liu, H.J. Fang, Y.L. Dai, L. Li, X.C. Xu, Y. Yan, K. Yu, Int. J. Electrochem. Sci. 13 (11) (2018) 11180–11192, doi:10.20964/2018.11.89.
[119] Y.W.X. Zhang, L. Han, L.B. Ren, L.L. Fan, Y.Y. Guo, M.Y. Zhou, G.F. Quan, T. Nonferr. Metal. Soc. 32 (8) (2022) 2510–2526, doi:10.1016/S1003-6326(22)65962-4.
[120] X.R. Chen, Y.H. Jia, Q.C. Le, H.N. Wang, X. Zhou, F.X. Yu, A. Atrens, J. Magnes. Alloy. 9 (6) (2021) 2113–2121, doi:10.1016/j.jma.2020.07.008.
[121] Y. Song, D.B. Su, Q. Yang, M. Yuan, B. Jiang, L.F. Jiang, F.S. Pan, J. Electrochem. Soc. 168 (9) (2021) 090526, doi:10.1149/1945-7111/ac227f.
[122] X.R. Chen, J. Venezuela, Z.M. Shi, Q.C. Le, M. Dargusch, Mater. Today. Energy. 36 (2023) 101363, doi:10.1016/j.mtener.2023.101363.
[123] X. Liu, Z.C. Guo, J.L. Xue, P.J. Zhang, Int. J. Energy. Res. 43 (9) (2019) 4569–4579, doi:10.1002/er.4586.
[124] X. Liu, J.L. Xue, P.J. Zhang, Z.J. Wang, J. Power. Sources. 414 (2019) 174–182, doi:10.1016/j.jpowsour.2018.12.092.
[125] N.T. Kirkland, N. Birbilis, J. Walker, T. Woodfield, G.J. Dias, M.P. Staiger, J. Biomed. Mater. Res. A 95B (1) (2010) 91–100, doi:10.1002/jbm.b.31687.
[126] S.B. Li, H. Li, C.C. Zhao, Z.H. Wang, K. Liu, W.B. Du, Electroana. Chem. 904 (2022) 115944, doi:10.1016/j.jelechem.2021.115944.
[127] X. Liu, J.L. Xue, Energy 189 (2019) 116314, doi:10.1016/j.energy.2019.116314.
[128] Q. Li, W. Xiong, S.R. Yu, Y. Liu, J. Li, L. Liu, X.J. Bi, G. Zhu, E.Y. Liu, Y. Zhao, B.Y. Wang, J. Mate. Sci. 56 (22) (2021) 12789–12802, doi:10.1007/s10853-021-06135-2.
[129] O.I. Malyi, T.L. Tan, S. Manzhos, J. Power. Sources. 233 (2013) 341–345, doi:10.1016/j.jpowsour.2013.01.114.

[130] S.Q. Yuan, H.M. Lu, Z.G. Sun, L. Fan, X.Y. Zhu, W. Zhang, J. Electrochem. Soc. 163 (7) (2016) A1181, doi:10.1149/2.0371607jes.
[131] J.L. Ma, J.B. Wen, F.Z. Ren, G.X. Wang, Y. Xiong, J. Electrochem. Soc. 163 (8) (2016) A1759, doi:10.1149/2.1241608jes.
[132] Q. Zou, Q.C. Le, X.R. Chen, Y.H. Jia, C.Y. Ban, T. Wang, H.N. Wang, R.Z. Guo, L. Ren, A. Atrens, Electrochim. Acta. 401 (2022) 139372, doi:10.1016/j.electacta.2021.139372.
[133] X.R. Chen, X. Liu, Q.C. Le, M.X. Zhang, M. Liu, A. Atrens, J. Mater. Chem. A. 9 (21) (2021) 12367–12399, doi:10.1039/D1TA01471D.
[134] X. Liu, S.Z. Liu, J.L. Xue, J. Power. Sources. 396 (2018) 667–674, doi:10.1016/j.jpowsour.2018.06.085.
[135] H.J. Zhang, D.Y. Ding, M.F. Tang, B. Song, Y.B. Niu, H.W. Dong, S.F. Guo, F.S. Pan, J. Alloy. Compd. 939 (2023) 168764, doi:10.1016/j.jallcom.2023.168764.
[136] Y.B. Ma, N. Li, D.Y. Li, M.L. Zhang, X.M. Huang, J. Power. Sources. 196 (4) (2011) 2346–2350, doi:10.1016/j.jpowsour.2010.07.097.
[137] N.G. Wang, R.C. Wang, Y. Feng, W.H. Xiong, J.C. Zhang, M. Deng, Corros. Sci. 112 (2016) 13–24, doi:10.1016/j.corsci.2016.07.002.
[138] Y.Z. Lv, M. Liu, Y. Xu, D.X. Cao, J. Feng, J. Power. Sources. 225 (2013) 124–128, doi:10.1016/j.jpowsour.2012.09.088.
[139] M.C. Lin, C.Y. Tsai, J.Y. Uan, Corros. Sci. 51 (10) (2009) 2463–2472, doi:10.1016/j.corsci.2009.06.036.
[140] Y. Tang, Q.C. Le, R.D.K. Misra, G.Q. Su, J.Z. Cui, Mater. Sci. Eng: A. 712 (2018) 266–280, doi:10.1016/j.msea.2017.11.114.
[141] X. Liu, J.L. Xue, S.Z. Liu, Mater. Design. 160 (2018) 138–146, doi:10.1016/j.matdes.2018.09.011.
[142] C.P. Li, Y.B. He, H.P. Huang, J. Magnes. Alloy. 9 (2) (2021) 569–580, doi:10.1016/j.jma.2020.02.022.
[143] T. Zhang, G.Z. Meng, Y.W. Shao, Z.Y. Cui, F.H. Wang, Corros. Sci. 53 (9) (2011) 2934–2942, doi:10.1016/j.corsci.2011.05.035.
[144] L.H. Li, W.H. Liu, F.G. Qi, D. Wu, Z.Q. Zhang, J. Magnes. Alloy. 10 (9) (2022) 2334–2353, doi:10.1016/j.jma.2022.09.003.
[145] G.S. Huang, Y.C. Zhao, Y.X. Wang, H. Zhang, F.S. Pan, Mater. Lett. 113 (2013) 46–49, doi:10.1016/j.matlet.2013.09.041.
[146] E. Gerashi, R. Alizadeh, T.G. Langdon, J. Magnes. Alloy. 10 (2) (2022) 313–325, doi:10.1016/j.jma.2021.09.009.
[147] Y.C. Shi, C.Q. Peng, Y. Feng, R.C. Wang, N.G. Wang, J. Alloy. Compd. 721 (2017) 392–404, doi:10.1016/j.jallcom.2017.05.267.
[148] R. Ueji, N. Tsuchida, D. Terada, N. Tsuji, Y. Tanaka, A. Takemura, K. Kunishige, Scripta. Mater. 59 (9) (2008) 963–966, doi:10.1016/j.scriptamat.2008.06.050.
[149] G. Dini, R. Ueji, Steel. Res. Int. 83 (4) (2012) 374–378, doi:10.1002/srin.201100308.
[150] R.L. Penn, J.F. Banfield, Science 281 (5379) (1998) 969–971, doi:10.1126/science.281.5379.969.
[151] D.Q. Wan, J.C. Wang, G.F. Wang, L. Lin, Z.G. Feng. G.C. Yang, Acta. Metall. Sin-Engl. 22 (1) (2009) 1–6, doi:10.1016/S1006-7191(08)60063-0.
[152] M. Uwaha, Prog. Cryst. Growth. Ch. 62 (2) (2016) 58–68, doi:10.1016/j.pcrysgrow.2016.04.002.
[153] Z.S. You, L. Lu, K. Lu, Acta. Mater. 59 (18) (2011) 6927–6937, doi:10.1016/j.actamat.2011.07.044.
[154] Q. Xiang, B. Jiang, Y.X. Zhang, X.B. Chen, J.F. Song, J.Y. Xu, L. Fang, F.S. Pan, Corros. Sci. 119 (2017) 14–22, doi:10.1016/j.corsci.2017.02.009.
[155] K. Hagihara, A. Kinoshita, Y. Sugino, M. Yamasaki, Y. Kawamura, H.Y. Yasuda, Y. Umakoshi, Acta. Mater. 58 (19) (2010) 6282–6293, doi:10.1016/j.actamat.2010.07.050.
[156] Y.M. Zhu, A.J. Morton, J.F. Nie, Acta. Mater. 60 (19) (2012) 6562–6572, doi:10.1016/j.actamat.2012.08.022.
[157] H. Liu, H. Huang, C. Wang, J. Sun, J. Bai, F. Xue, A. Ma, X.B. Chen, JOM. 71 (9) (2019) 3314–3327, doi:10.1007/s11837-019-03610-9.
[158] H.J. Zhang, D.Y. Ding, C. Su, B. Song, N. Guo, S.F. Guo, J. Mater. Sci. 58 (36) (2023) 14452–14466, doi:10.1007/s10853-023-08922-5.
[159] X.R. Chen, H.N. Wang, Q. Zou, Q.C. Le, C.E. Wen, A. Atrens, Electrochim. Acta. 367 (2021) 137518, doi:10.1016/j.electacta.2020.137518.
[160] X. Zhao, L.L. Shi, J. Xu, Mater. Sci. Eng: C. 33 (7) (2013) 3627–3637, doi:10.1016/j.msec.2013.04.051.
[161] C.Q. Li, D.K. Xu, Z.R. Zeng, B.J. Wang, L.Y. Sheng, X.B. Chen, E.H. Han, Mater. Design. 121 (2017) 430–441, doi:10.1016/j.matdes.2017.02.078.
[162] X.R. Chen, H.N. Wang, Q.C. Le, Y.H. Jia, X. Zhou, F.X. Yu, A. Atrens, Int. J. Energ. Res. 44 (11) (2020) 8865–8876, doi:10.1002/er.5595.
[163] R. Davidson, A. Verma, D. Santos, F. Hao, C.D. Fincher, D. Zhao, V. Attari, P. Schofield, J.V. Buskirk, A. Fraticelli-Cartagena, T.E.G. Alivio, R. Arroyave, K. Xie, M. Pharr, P.P. Mukherjee, S. Banerjee, Mater. Horiz. 7 (3) (2020) 843–854, doi:10.1039/C9MH01367A.
[164] C. Ling, D. Banerjee, M. Matsui, Electrochim. Acta. 76 (2012) 270–274, doi:10.1016/j.electacta.2012.05.001.
[165] R. Davidson, A. Verma, D. Santos, F. Hao, C. Fincher, S. Xiang, J.V. Buskirk, K. Xie, M. Pharr, P.P. Mukherjee, S. Banerjee, ACS. Energy. Lett. 4 (2) (2019) 375–376, doi:10.1021/acsenergylett.8b02470.
[166] M. Jäckle, A. Groß, J. Chem. Phys. 141 (17) (2014) 174710, doi:10.1063/1.4901055.
[167] M.S. Ding, T. Diemant, R.J. Behm, S. Passerini, G.A. Giffin, J. Electrochem. Soc. 165 (10) (2018) A1983, doi:10.1149/2.1471809jes.
[168] J.H. Kwak, Y. Jeoun, S.H. Oh, S. Yu, J.H. Lim, Y.E. Sung, S.H. Yu, H.D. Lim, ACS. Energy. Lett. 7 (1) (2022) 162–170, doi:10.1021/acsenergylett.1c02486.
[169] W. Wang, J.J. Liu, T.Q. Wu, T.X. Mao, J.P. Chen, W.C. Zhang, Z.C. Shi, N.G. Wang, J. Power. Sources. 583 (2023) 233569, doi:10.1016/j.jpowsour.2023.233569.
[170] N.G. Wang, R.C. Wang, C.Q. Peng, Y. Feng, Corros. Sci. 81 (2014) 85–95, doi:10.1016/j.corsci.2013.12.005.
[171] J.L. Wu, R.C. Wang, Y. Feng, C.Q. Peng, J. Alloy. Compd. 765 (2018) 736–746, doi:10.1016/j.jallcom.2018.05.070.
[172] Y. Song, K. Yao, Q. Zou, Q. Yang, B. Jiang, L.D. Wang, M. Yuan, Q.H. Wang, G.S. Huang, F.S. Pan, J. Electrochem. Soc. 169 (2) (2022) 020575, doi:10.1016/j.jma.2023.08.009.
[173] N.G. Wang, Y.C. Mu, Q. Li, Z.C. Shi, RSC. Adv. 7 (84) (2017) 53226–53235, doi:10.1039/c7ra10652a.
[174] F. Shangguan, W.L. Cheng, Y.H. Chen, H. Yu, L.F. Wang, H. Li, H.X. Wang, J.H. Wang, J. Power. Sources. 564 (2023) 232856, doi:10.1016/j.jpowsour.2023.232856.
[175] M. Yuasa, X. Huang, K. Suzuki, M. Mabuchi, Y. Chino, Mater. Trans. 55 (8) (2014) 1202–1207, doi:10.2320/matertrans.MC201403.
[176] X.R. Chen, Q. Zou, Q.C. Le, M.X. Zhang, M. Liu, A. Atrens, Chem. Eng. J. 433 (2022) 133797, doi:10.1016/j.cej.2021.133797.
[177] D.Y. Ding, Y.H. Du, M.F. Tang, B. Song, N. Guo, H.J. Zhang, S.F. Guo, T. Nonferr. Metal. Soc. 33 (7) (2023) 2014–2029, doi:10.1016/S1003-6326(23)66240-5.
[178] Z. Han, W. Xu, C.B. Liu, L.Y. Cui, R.C. Zeng, J. Mater. Res. Technol. 25 (2023) 7024–7038, doi:10.1016/j.jmrt.2023.07.122.
[179] H.Q. Xiong, K. Yu, X. Yin, Y.L. Dai, Y. Yan, H.L. Zhu, J. Alloy. Compd. 708 (2017) 652–661, doi:10.1016/j.jallcom.2016.12.172.
[180] A. Alamo, A.D. Banchik, J. Mate. Sci. 15 (1) (1980) 222–229, doi:10.1007/BF00552448.
[181] D.Y. Huang, F.Y. Cao, T. Ying, D.J. Zheng, G.L. Song, J. Power. Sources. 520 (2022) 230874, doi:10.1016/j.jpowsour.2021.230874.
[182] S.K. Wei, Z.H. Han, Y. Xu, L. Xu, J. Mater. Sci. 58 (30) (2023) 12433–12449, doi:10.1007/s10853-023-08784-x.
[183] N.G. Wang, W.P. Li, Y.X. Huang, G. Wu, M.C. Hu, G.Z. Li, Z.C. Shi, J. Power. Sources. 436 (2019) 226855, doi:10.1016/j.jpowsour.2019.226855.
[184] D. Aurbach, I. Weissman, Y. Gofer, E. Levi, Chem. Rec. 3 (1) (2003) 61–73 doi: 10.1002/tcr.10051.
[185] K.F. Blurton, A.F. Sammells, J. Power. Sources. 4 (4) (1979) 263–279, doi:10.1016/0378-7753(79)80001-4.
[186] Y.L. Liang, R.J. Feng, S.Q. Yang, H. Ma, J. Liang, J. Chen, Adv. Mater. 23 (5) (2011) 640–643, doi:10.1002/adma.201003560.